



Published in final edited form as:

Nature. 2021 January ; 589(7842): 474–479. doi:10.1038/s41586-020-3008-z.

A Non-Hallucinogenic Psychedelic Analog with Therapeutic Potential

Lindsay P. Cameron¹, Robert J. Tombari², Ju Lu³, Alexander J. Pell², Zefan Q. Hurley², Yann Ehinger⁴, Maxemiliano V. Vargas¹, Matthew N. McCarroll⁵, Jack C. Taylor⁵, Douglas Myers-Turnbull^{5,6}, Taohui Liu³, Bianca Yaghoobi⁷, Lauren J. Laskowski⁸, Emilie I. Anderson⁸, Guoliang Zhang², Jayashri Viswanathan², Brandon M. Brown⁹, Michelle Tjia³, Lee E. Dunlap², Zachary T. Rabow¹⁰, Oliver Fiehn¹⁰, Heike Wulff⁹, John D. McCorvy⁸, Pamela J. Lein⁷, David Kokel^{5,11}, Dorit Ron⁴, Jamie Peters^{12,13}, Yi Zuo³, David E. Olson^{2,14,15,16,*}

¹Neuroscience Graduate Program, University of California, Davis, Davis, CA 95618, USA

²Department of Chemistry, University of California, Davis, One Shields Avenue, Davis, CA 95616, USA

³Department of Molecular, Cell & Developmental Biology, University of California, Santa Cruz, 1156 High Street, Santa Cruz, CA 95064, USA

⁴Department of Neurology, University of California, San Francisco, 675 Nelson Rising Lane, San Francisco, CA 94143, USA

⁵Institute for Neurodegenerative Diseases, University of California, San Francisco, San Francisco, CA 94143, USA

⁶Quantitative Biosciences Consortium, University of California, San Francisco, San Francisco, CA 94143, USA

⁷Department of Molecular Biosciences, School of Veterinary Medicine, University of California, Davis, 1089 Veterinary Medicine Drive, Davis, CA 95616, USA

Users may view, print, copy, and download text and data-mine the content in such documents, for the purposes of academic research, subject always to the full Conditions of use:http://www.nature.com/authors/editorial_policies/license.html#terms

*Corresponding author: deolson@ucdavis.edu.

Author Contributions

AJP, ZQH, and GZ synthesized the ibogalogs. LED synthesized 5-MeO-DMT fumarate and performed the CNS MPO calculations. LPC performed the dendritogenesis and spinogenesis assays. LPC and JV performed the head-twitch response experiments. MNM performed the zebrafish heart rate and seizure experiments. JCT, DM-T, and RJT performed the zebrafish behavioral experiments. RJT and BY performed the zebrafish toxicity assays. BMB and LPC performed the hERG inhibition studies. LPC performed the solubility studies and CPP experiments. JL, TL, and LPC performed the experiments assessing in vivo spine dynamics. LJM, EIA, and JDM performed the receptor functional assays. JL and MT performed the forced swim test following UMS. MVV performed the forced swim test study without UMS with assistance from LED. ZTR and LPC performed the pharmacokinetic studies. JP performed the heroin self-administration experiments. YE performed the alcohol consumption assays. LPC performed the sucrose preference assay. OF, HW, JDM, PJJ, DK, DR, JP, YZ, and DEO supervised various aspects of this project and assisted with data analysis. DEO conceived the project and wrote the manuscript with input from all authors.

Disclosure

DEO is the president and chief scientific officer of Delix Therapeutics, Inc. Delix Therapeutics has licensed TBG-related technology from the University of California, Davis.

Code Availability

Custom written data analysis codes are available upon request.

⁸Department of Cell Biology, Neurobiology, and Anatomy, Medical College of Wisconsin, 8701 Watertown Plank Road, Milwaukee, WI 53226, USA

⁹Department of Pharmacology, School of Medicine, University of California, Davis, 451 Health Sciences Drive, Suite 3503, Davis, CA 95616, USA

¹⁰West Coast Metabolomics Center, University of California, Davis, One Shields Avenue, Davis, CA 95616, USA

¹¹Department of Physiology, University of California, San Francisco, San Francisco, CA 94158, USA

¹²Department of Anesthesiology, University of Colorado Denver, Anschutz Medical Campus, Aurora, CO, 80045, USA

¹³Department of Pharmacology, University of Colorado Denver, Anschutz Medical Campus, Aurora, CO, 80045, USA

¹⁴Department of Biochemistry & Molecular Medicine, School of Medicine, University of California, Davis, 2700 Stockton Blvd, Suite 2102, Sacramento, CA 95817, USA

¹⁵Center for Neuroscience, University of California, Davis, 1544 Newton Ct, Davis, CA 95618, USA

¹⁶Delix Therapeutics, Inc., 853 Alma St., Palo Alto, CA 94301, USA

Abstract

The psychedelic alkaloid ibogaine has anti-addictive properties in both humans and animals.¹ Unlike most substance use disorder (SUD) medications, anecdotal reports suggest that ibogaine possesses the potential to treat patients addicted to a variety of substances including opiates, alcohol, and psychostimulants. Like other psychedelic compounds, its therapeutic effects are long-lasting,² which has been attributed to its ability to modify addiction-related neural circuitry through activation of neurotrophic factor signaling.^{3,4} However, several safety concerns have hindered the clinical development of ibogaine including its toxicity, hallucinogenic potential, and proclivity for inducing cardiac arrhythmias. Here, we apply the principles of function-oriented synthesis (FOS) to identify the key structural elements of its potential therapeutic pharmacophore, enabling us to engineer tabernanthalog (TBG)—a water soluble, non-hallucinogenic, non-toxic analog of ibogaine that can be prepared in a single step. TBG promoted structural neural plasticity, reduced alcohol- and heroin-seeking behavior, and produced antidepressant-like effects in rodents. This work demonstrates that through careful chemical design, it is possible to modify a psychedelic compound to produce a safer, non-hallucinogenic variant with therapeutic potential.

Keywords

psychedelic; psychoplastogen; neural plasticity; ibogaine; function-oriented synthesis; drug design; neuropsychiatric disorder; substance use disorder; addiction; alcohol use disorder; opioid use disorder; antidepressant; depression; serotonin; 5-HT_{2A} receptor

Ibogaine is the most abundant of the numerous alkaloids produced by *Tabernanthe iboga*,⁵ and though it has not been tested in double-blind placebo-controlled clinical trials, anecdotal reports and open-label studies suggest that it can reduce symptoms of drug withdrawal, reduce drug cravings, and prevent relapse.^{1,6} Unfortunately, ibogaine suffers from major issues that severely limit its potential as a therapeutic. First, access to large quantities has been limited by overexploitation of the plant from which it is derived as well as the lack of a scalable, enantioselective, total synthesis.⁶ Currently, there are only three synthetic routes to racemic ibogaine with longest linear sequences of 9–16 steps and overall yields ranging from 0.1–4.8%.⁶ Second, ibogaine's safety profile is unacceptable. From a physicochemical perspective, it is very non-polar, which leads to its accumulation in adipose tissue⁷ and contributes to its known cardiotoxicity through inhibition of hERG potassium channels.^{8,9} Several deaths have been linked to ibogaine's cardiotoxicity,^{10,11} and it produces long-lasting hallucinations (> 24 h). While ibogaine was once sold in France as a medicine for treating neuropsychiatric diseases, it was removed from the market due to its adverse effects.

Though ibogaine's exact mechanism of action has not yet been fully elucidated, evidence suggests that it might alter addiction-related circuitry by promoting neural plasticity. First, ibogaine has been shown to increase glial cell line-derived neurotrophic factor (GDNF) expression in the ventral tegmental area (VTA), and intra-VTA infusion of ibogaine reduces alcohol-seeking behavior in rodents.³ A more recent study demonstrated that ibogaine impacts brain-derived neurotrophic factor (BDNF) and GDNF signaling in multiple brain regions implicated in the behavioural effects of addictive drugs.⁴ Recently, we demonstrated that noribogaine, an active metabolite of ibogaine,¹² is a potent psychoplastogen¹³ that increases cortical neuron dendritic arbor complexity.¹⁴ Other psychoplastogens, such as lysergic acid diethylamide (LSD) and psilocin (the active metabolite of psilocybin) have also been shown in anecdotal and open-label studies to decrease drug use in the clinic, similar to ibogaine.¹⁵ We hypothesize that the ability of psychoplastogens to promote structural and functional neural plasticity in addiction-related circuitry might explain their abilities to reduce drug-seeking behavior for weeks to months following a single administration. Moreover, by modifying neural circuitry rather than simply blocking the targets of a particular addictive substance, psychoplastogens like ibogaine could have the potential to be broadly applicable anti-addictive agents.

In order to develop simplified, and potentially safer analogs, we first needed to understand which of ibogaine's structural features were critical for its psychoplastogenic effects. Our approach mirrored that taken by Wender and colleagues in their seminal FOS studies on the structurally complex marine natural product bryostatin 1.¹⁶ Here, we report our efforts to engineer simplified analogs of iboga alkaloids (ibogalogs) that lack ibogaine's toxicity and hallucinogenic effects but maintain its behavioural effects in rodent models of drug self-administration and relapse.

Function-Oriented Synthesis of Ibogalogs

The hallmarks of ibogaine's structure include an indole, a 7-membered tetrahydroazepine, and a bicyclic isoquinuclidine (Fig. 1). We reasoned that systematic deletion of these key

structural elements would reveal the essential features of ibogaine's psychoplastogenic pharmacophore. By adapting chemistry developed by Sames and co-workers,¹⁷ we were able to access a series of isoquinuclidine-containing compounds (**8–11**) that lacked the tetrahydroazepine and/or indole characteristic of ibogaine (Extended Data Fig. 1a). Ibogalog **8a** lacks both the indole and tetrahydroazepine rings characteristic of ibogaine, while **9a–11a** only lack the tetrahydroazepine. Ibogamine, ibogaine, and noribogaine only differ from **9a**, **10a**, and **11a** by the presence of the C2–C16 bond (LeMen and Taylor convention), respectively.

Key Structural Elements of Ibogaine's Psychoplastogenic Pharmacophore

Except for **11a**, ibogalogs containing the isoquinuclidine but lacking the tetrahydroazepine ring (**8–10** and **11b**) were either weak psychoplastogens or did not promote neuronal growth compared to the vehicle (VEH) control (Extended Data Fig. 2). In contrast, the majority of ibogalogs lacking the isoquinuclidine but retaining the tetrahydroazepine (**12–16**) were efficacious (Extended Data Fig. 2). Indole substitution at C5 with either fluorine (**15**) or chlorine (**16**) was tolerated, but a more sterically demanding bromine substituent (**17**) was not. We found that IBG (**13**) performed comparably to ibogaine despite having a simplified chemical structure. We prioritized IBG for further development as we reasoned that its reduced lipophilicity (cLogP = 2.61) relative to ibogaine (cLogP = 4.27) would make formulation less challenging and also reduce the potential for cardiotoxicity, as lipophilicity is a known contributing factor to hERG channel inhibition. The attractiveness of IBG as a potential therapeutic was underscored by its improved CNS multiparameter optimization (MPO) score¹⁸ (IBG MPO = 5.2; Ibogaine MPO = 3.8; optimal MPO = 6.0) coupled with the fact that it can be synthesized in a single step.

TBG is a Safer, Non-Hallucinogenic 5-HT2A Agonist

Inspection of IBG's structure reveals its similarity to the potent hallucinogen and 5-HT2A agonist 5-methoxy-*N,N*-dimethyltryptamine (5-MeO-DMT). Pioneering structure-activity relationship (SAR) studies conducted by Glennon and co-workers demonstrated that, unlike 5-MeO-DMT and other known hallucinogens, 6-MeO-DMT did not substitute for the hallucinogen 2,5-dimethoxy-4-methylamphetamine (DOM) at any dose in rodents trained to discriminate DOM from saline.¹⁹ Moreover, our group has shown that 6-MeO-DMT does not produce a head-twitch response (HTR)²⁰—a well-established rodent behavioral proxy for hallucinations induced by 5-HT2A agonists.²¹ Therefore, we synthesized the 6-methoxyindole-fused tetrahydroazepine **18**. As **18** resembles the iboga alkaloid tabernanthine, we refer to this compound as tabernanthalog (TBG). Like IBG, TBG can be synthesized in a single step enabling us to rapidly access large quantities (>1 g).

To evaluate the hallucinogenic potential of IBG and TBG, we tested them in the HTR assay using 5-MeO-DMT (10 mg/kg) as a positive control (Fig. 2a). While 5-MeO-DMT produces a robust HTR, its conformationally restricted analog IBG exhibits significantly reduced hallucinogenic potential. As hypothesized, the 6-methoxy substituent of TBG rendered it devoid of hallucinogenic potential as measured by the HTR assay. For these in vivo studies,

we used the fumarate salts of IBG and TBG. Unlike ibogaine hydrochloride, they are readily soluble in 0.9% saline up to 40 mg/mL (Extended Data Table 1).

The lipophilicity of ibogaine not only poses practical issues for its administration, it is likely a major factor contributing to its toxicity and adverse cardiac effects. Ibogaine inhibits hERG channels with an IC_{50} of 1 μ M (Fig. 2b). In contrast, IBG and TBG are approximately 10- and 100-fold less potent than ibogaine, respectively, indicating a lower potential for cardiotoxicity. Administration of ibogaine to immobilized larval zebrafish decreased heart rate (Extended Data 3a, Video S1) and increased the likelihood for inducing arrhythmias as measured by the ratio of atrium to ventricle beats per minute (BPM) (Fig. 2c). Neither IBG nor TBG induced these undesirable phenotypes.

To compare the acute behavioral effects of ibogaine, IBG, and TBG, we treated larval zebrafish with these compounds across a range of doses (1–200 μ M), recorded their behavioral responses to a battery of light and acoustic stimuli,^{20,22} and analyzed the resulting behavioral profiles (Extended Data 3b). Treatment with ibogaine and noribogaine produced behavioral profiles similar to the lethal control (Extended Data 3b–c). In contrast, IBG- and TBG-treated zebrafish produced behavioral profiles more similar to the vehicle control. With increasing concentration, ibogaine, noribogaine, and the hERG inhibitors haloperidol, sertindole, and terfenadine become more phenotypically distinct from the vehicle control, while more closely resembling the lethal control (eugenol, 100 μ M) (Extended Data 3d). In contrast, IBG and TBG did not produce this phenotype.

As it is unclear whether or not ibogaine causes seizures at very high doses,^{1,23} we next used larval zebrafish expressing GCaMP5 to assess seizurogenic potential. Neither ibogaine nor TBG produced excessive neural activity as was observed following treatment with the known seizure-inducing compound pentylenetetrazole (PTZ) (Extended Data 3e, Video S2).

Finally, we compared the morphological effects of ibogaine, IBG, and TBG using a well-established zebrafish developmental toxicity assay.²⁴ Ibogaine (100 μ M) significantly increased malformations and mortality at 2 and 5 days post-fertilization (dpf), respectively (Fig. 2d–e). At both timepoints, the proportion of viable to non-viable fish was significantly different from vehicle control ($p < 0.0001$). Ibogaine-treated zebrafish suffered from numerous malformations. Noribogaine treatment resulted in greater survival, but the majority of zebrafish exhibited yolk sac and/or pericardial edemas. In contrast, both IBG and TBG treatments (100 μ M) resulted in significantly fewer non-viable fish than ibogaine ($p < 0.0001$ for ibogaine vs. IBG and ibogaine vs. TBG at both 2 and 5 dpf). Importantly, reducing the concentration of TBG from 100 to 66 μ M resulted in a proportion of viable to non-viable fish that was statistically indistinguishable from vehicle control after 5 dpf ($p = 0.3864$, Extended Data 3f).

To validate the targets of IBG and TBG, we performed a panel of serotonin (5-HT) and opioid receptor functional assays assessing canonical GPCR signaling. Unlike noribogaine, IBG and TBG showed weak or no opioid agonist activity (Extended Data Figs. 4 and 5). However, IBG and TBG demonstrated potent agonist activity at human (Fig. 2f) and mouse 5-HT_{2A} receptors (Extended Data Fig. 4). Many 5-HT_{2A} agonists, such as 5-MeO-DMT,

are also agonists of 5-HT_{2B} receptors, which can lead to cardiac valvulopathy.²⁵ In contrast, IBG and TBG act as antagonists at 5-HT_{2B} receptors (Fig. 2f). When profiled across the 5-HT receptorome, both IBG and TBG displayed more selective, and potentially safer profiles as compared to the less conformationally restricted 5-MeO-DMT (Extended Data Figs. 4 and 5). A full safety screen across 81 potential targets revealed that TBG exhibits high selectivity for 5-HT₂ receptors (Extended Data Table 2).

To determine if TBG has rewarding effects, we performed a conditioned place preference assay (CPP) in mice (Extended Data Fig. 6). A low dose of TBG (1 mg/kg) did not have any effect on place preference ($p = 0.8972$). Higher doses produced a modest conditioned place aversion (CPA) ($p = 0.0199$ for 10 mg/kg; $p = 0.0489$ for 50 mg/kg), suggesting that TBG has a low potential for abuse.

Effect of TBG on Neural Plasticity

Having demonstrated the improved safety profile of TBG relative to ibogaine, we next assessed its effects on structural plasticity. Treating rat embryonic cortical neurons with TBG increased dendritic arbor complexity as measured by Sholl analysis (Fig. 3a), and this effect appears to be 5-HT_{2A}-dependent, as it was blocked by pretreatment with the 5-HT_{2A} antagonist ketanserin (Fig. 3b).

In addition to promoting dendritic growth, TBG also increases dendritic spine density to a comparable extent as ibogaine in mature cortical cultures (DIV20) (Fig. 3c–d). Next, we used transcranial 2-photon imaging (Fig. 3e) to assess the effects of TBG on spine dynamics in mouse sensory cortex. Both TBG and the hallucinogenic 5-HT_{2A} agonist 2,5-dimethoxy-4-iodoamphetamine (DOI) increased spine formation without impacting spine elimination 24 h after treatment (Fig. 3f–g). Similar results were observed in more anterior parts of the cortex and mirrored the effects of ketamine reported previously.²⁶

Effect of TBG on Forced Swim Test Behavior After Stress

As increased structural plasticity in the anterior parts of the brain (e.g. prefrontal cortex, PFC) have been shown to mediate the sustained (>24 h) antidepressant-like effects of ketamine²⁷ in rodent models and are hypothesized to play a key role in the therapeutic effects of 5-HT_{2A} agonists,^{14,28} we next evaluated the impact of TBG on forced swim test (FST) behavior following 7 days of unpredictable mild stress (UMS) (Extended Data Fig. 7a–b) in mice. Immobility time was significantly increased after UMS. This effect was rescued by a 50 mg/kg, but not 10 mg/kg, dose of TBG. Preliminary pharmacokinetic studies revealed that a 50 mg/kg dose of TBG produced significantly higher brain concentrations than did a 10 mg/kg dose (Extended Data Fig. 7c). Therefore, the 50 mg/kg dose was used in subsequent mouse behavioral experiments.

As ketamine produces antidepressant-like effects in the FST even in the absence of UMS, we performed a head-to-head comparison with TBG in this experiment (Fig. 4a–b). Drugs were administered 24 h after a pre-test, and the FST was performed 24 h and 7 d post drug administration. Both ketamine and TBG significantly reduced immobility in mice 24 h following drug administration, however, ketamine's effects appeared to be more durable.

Importantly, TBG had no effect on locomotion 24 h following administration (Extended Data Fig. 6c). As anticipated, treatment with a 5-HT_{2A} antagonist (ketanserin) blocked the antidepressant-like effect of TBG (Fig. 4b). The efficacy exhibited by TBG in the FST is consistent with the fact that other 5-HT_{2A} agonists have demonstrated potential for treating depression.^{13,28} However, future studies should evaluate the effects of TBG on other behaviors relevant to depression, particularly those measuring anhedonia.

Effect of TBG on Alcohol- and Heroin-Seeking Behavior

To assess the effect of TBG on alcohol (EtOH) intake, we employed an intermittent access 2-bottle choice (20% EtOH (v/v) vs. H₂O) experiment that models binge drinking behavior in humans.²⁹ Mice were subjected to repeated cycles of binge drinking and withdrawal over the course of 7 weeks (Fig. 4c), which resulted in high EtOH consumption (11.44 ± 0.76 g/kg/24h), binge drinking-like behavior (3.89 ± 0.33 g/kg/4h), and generated blood alcohol content equivalent to that of human subjects suffering from alcohol use disorder (AUD). Systemic injections of TBG 3 h prior to a drinking session reduced binge drinking during the first 4 h without affecting water intake (Fig. 4d). Consumption of alcohol was lower for at least two days following TBG administration (Fig. 4e). Similar results were observed previously for ibogaine.³ Importantly, administration of TBG prior to giving mice access to both water and a 5% sucrose solution did not decrease sucrose preference (Fig. 4f) or total fluid consumption (Fig. 4g), indicating that TBG selectively reduced alcohol intake.

As with alcohol consumption, anecdotal reports suggest that ibogaine can reduce opioid use in humans.^{1,6} In rodent models of opioid self-administration, ibogaine produces the greatest decrease when administered at a dose of 40 mg/kg.³⁰ Here, we used a rat model of heroin self-administration (Fig. 4h) to assess the effects of TBG (40 mg/kg) administered during three distinct epochs—during self-administration (SA), prior to the first day of extinction (EXT), and immediately before cued reinstatement (CUE). Vehicle was administered at these same time points whenever TBG was not (Fig. 4i). Thus, each group received a total of 3 injections. When administered during self-administration (Fig. 4j–k), immediately prior to extinction (EXT, Fig. 4l) or before cued reinstatement (CUE, Fig. 4m), TBG acutely reduced heroin-seeking behavior. While TBG did not induce any acute locomotor deficits (Extended Data Fig. 8a), the acute effects of TBG should be interpreted with caution. Similar to heroin, acute TBG administration strongly reduced sucrose self-administration at all three timepoints (Extended Data Fig. 8b–e), indicating that the acute effects of TBG may be due to non-selective disruption of operant responding.

Strikingly, cue-induced relapse was reduced in the groups that had received TBG treatment long before cued reinstatement (SA and EXT, Fig. 4m). In sharp contrast, TBG had no impact on cued reinstatement of sucrose-seeking behavior when administered 12–14 days prior (Extended Data Fig. 8e). Thus, a single administration of TBG elicited anti-addictive effects lasting up to 12–14 days. Long-lasting protections against relapse after a single treatment have rarely been reported, but they are reminiscent of results in a cocaine self-administration model following direct injection of BDNF into the PFC.³¹

Discussion

Compounds capable of modifying neural circuits controlling motivation, anxiety, and drug-seeking behavior have been hypothesized to be effective treatments for a diverse range of neuropsychiatric disorders including depression, post-traumatic stress disorder, and SUD.¹³ In principle, such psychoplastogenic medicines could produce sustained therapeutic effects by rectifying underlying pathological changes in circuitry rather than masking disease symptoms. Psychedelic compounds may prove useful in this regard because they promote structural and functional neural plasticity in the PFC of rodents.¹⁴ While their putative therapeutic mechanisms of action are unknown, anecdotal reports and small clinical trials suggest that they might produce sustained therapeutic responses in multiple neuropsychiatric disorders following a single administration.

While psychedelics and ketamine have been hypothesized to share a common antidepressant mechanism of action related to cortical neuron growth in the PFC, a causal link between psychedelic-induced neuronal growth and behavior has yet to be established in either humans or rodents. In contrast, Liston and co-workers recently used a synapse targeting photoactivatable Rac1 to demonstrate that the sustained antidepressant-like effects of ketamine in mice are mediated in part by spinogenesis in the PFC.²⁷

Here, we used the principles of FOS to identify the indole-fused tetrahydroazepine as the key psychoplastogenic pharmacophore of ibogaine. This information enabled us to develop a 1-step synthesis of ibogaine analogs capable of promoting structural neural plasticity both in cell culture and in vivo. Simplification of ibogaine's architecture to produce TBG not only enhanced synthetic tractability; it also improved physicochemical properties and safety. Compounds lacking the isoquinuclidine were significantly less potent inhibitors of hERG channels and did not induce bradycardia or show signs of toxicity in zebrafish. With the exception of 18-methoxycoronaridine (18-MC), which is currently in phase II clinical trials, very few ibogaine analogs have demonstrated this level of safety while also producing therapeutic effects.³² It is unknown if 18-MC is psychoplastogenic, but unlike ibogaine, it does not increase *GDNF* expression in SH-SY5Y cells or reduce alcohol self-administration following direct infusion into the ventral tegmental area, suggesting their mechanisms of action are likely distinct.³³ While the synthesis of 18-MC is 13 steps,³⁴ TBG can be synthesized in a single step.

Not only does TBG potently promote neuronal growth, it also produces antidepressant-like behavioral responses and reduces alcohol (but not sucrose) consumption in mice. In rats, acute administration of TBG strongly inhibits both heroin- and sucrose-seeking behavior, likely by disrupting operant responding. However, when administered days in advance, TBG only prevents cued reinstatement of heroin-seeking behavior (but not sucrose). Future work is required to further characterize the optimal dosing regimen and time course for producing these behavioral effects in rodents, and to determine whether structural plasticity plays a causal role.

METHODS

Data Analysis and Statistics.

Treatments were randomized, and data were analyzed by experimenters blinded to treatment conditions. Statistical analyses were performed using GraphPad Prism (version 8.1.2) unless noted otherwise. All comparisons were planned prior to performing each experiment. Data are represented as mean \pm SEM, unless otherwise noted, with asterisks indicating * $p < 0.05$, ** $p < 0.01$, *** $p < 0.001$, and **** $p < 0.0001$. Boxplots depict the three quartile values of the distribution with whiskers extending to points that lie within 1.5 IQRs (interquartile range) of the lower and upper quartile. Observations falling outside this range are displayed independently. For Figs. 2a, 3a, 3b, 3d, 3g, 4b, Extended Data Fig. 2b, and Extended Data Fig. 7b, compound treatments were compared to the VEH control using a one-way ANOVA with Dunnett's post hoc test. For Extended Data 3a and Fig. 2c, time 0 h and time 1 h (before and after drug administration, respectively) data were compared using a paired t-test. For Extended Data 3f, compound treatments were compared using Fisher's exact test and p-values are indicated in the text. For Fig. 4d and Extended Data Fig. 6b, data were analyzed using a two-tailed paired t-test. Data in Fig. 4e–g and Extended Data Fig. 8a (distance and velocity) were analyzed using a two-way ANOVA with Sidak's post hoc test. For Fig. 4j, Fig. 4l–m, and Extended Data Fig. 8c–e, two-way repeated measures (RM) ANOVAs with treatment group as the between-subject factor and lever type (active versus inactive) as the within-subject factor were used. Sidak post-hoc tests were conducted as appropriate. For Extended Data Fig. 6c, a one-way ANOVA with Tukey's post hoc test was used. For Fig. 4k and Extended Data Fig. 8a (thigmotaxis) two-tailed unpaired t-tests were used.

Drugs.

The NIDA Drug Supply Program provided ibogaine hydrochloride (IBO), noribogaine (NOR), heroin (diamorphine hydrochloride), and cocaine hydrochloride. Other chemicals were purchased from commercial sources such as ketamine hydrochloride (KET, Fagron), ketanserin (KETS, ApexBio), eugenol (Tokyo Chemical Industries), and 5-hydroxytryptamine (Sigma-Aldrich). The fumarate salt of 5-methoxy-*N,N*-dimethyltryptamine (2:1, 5-MeO-DMT:fumaric acid) was synthesized in house as described previously²⁰ and judged to be analytically pure based on NMR and LC-MS data. For cell culture experiments, VEH = 0.1% (agonist studies) or 0.2% (antagonist studies) molecular biology grade dimethyl sulfoxide (Sigma-Aldrich). For in vivo experiments, VEH = USP grade saline (0.9%). Free bases were used for all cellular experiments while the fumarate salts of ibogainol and tabernanthol were used for the in vivo studies.

Animals.

All experimental procedures involving animals were approved by either the UCD, UCSF, UCSC or CU Anschutz Institutional Animal Care and Use Committee (IACUC) and adhered to principles described in the National Institutes of Health Guide for the Care and Use of Laboratory Animals. Power analyses were conducted to ensure appropriate sample size for all experiments involving animals. The University of California, Davis (UCD), the University of California, San Francisco (UCSF), the University of California, Santa Cruz (UCSC), and the University of Colorado Denver, Anschutz Medical Campus (CU Anschutz)

are accredited by the Association for Assessment and Accreditation of Laboratory Animal Care International (AAALAC).

Calculation of CNS MPO Score.

CNS MPO scores were calculated using a previously published method.¹⁸ Predicted pK_a values were determined using Marvin Sketch (19.25.0). LogP and total polar surface area were predicted using Molinspiration (<https://www.molinspiration.com/>). LogD was calculated using the following equation $\text{LogD} = \text{LogP} - \text{LOG}_{10}(1+10^{(\text{pka}-7.4)})$.

Dendritogenesis Experiments.

For the dendritogenesis experiments conducted using cultured cortical neurons, timed pregnant Sprague Dawley rats were obtained from Charles River Laboratories (Wilmington, MA). Full culturing, staining, and analysis details were performed as previously described.²⁰ Dendrites were visualized using a chicken anti-MAP2 antibody (1:10,000; EnCor, CPCA-MAP2) as previously reported.²⁰

Head-Twitch Response (HTR).

The head-twitch response assay was performed as described previously²⁰ using both male and female C57BL/6J mice (2 per treatment). The mice were obtained from Jackson Laboratory (Sacramento, C.A.) and were approximately 8 weeks old at the time of the experiments. Compounds were administered via intraperitoneal injection (5 mL/kg) using 0.9% saline as the vehicle. As a positive control, we utilized 5-MeO-DMT fumarate (2:1 amine/acid), which was synthesized as described previously.²⁰ Behavior was videotaped, later scored by two blinded observers, and the results were averaged (Pearson correlation coefficient = 0.93).

hERG Inhibition Studies.

All experiments were conducted manually using a HEKA EPC-10 amplifier at room temperature in the whole-cell mode of the patch-clamp technique. HEK293 cells stably expressing hKv11.1 (hERG) under G418 selection were a gift from Craig January (University of Wisconsin, Madison). Cells were cultured in DMEM containing 10% fetal bovine serum, 2 mM glutamine, 1 mM sodium pyruvate, 100 U/mL penicillin, 100 µg/mL streptomycin, and 500 mg/ml G418. The cell line was not authenticated or tested for mycoplasma contamination. Before experiments, cells were grown to 60–80% confluency, lifted using TrypLE, and plated onto poly-L-lysine-coated coverslips. Patch pipettes were pulled from soda lime glass (micro-hematocrit tubes) and had resistances of 2–4 MΩ. For the external solution, normal sodium Ringer was used (160 mM NaCl, 4.5 mM KCl, 2 mM CaCl₂, 1 mM MgCl₂, 10 mM HEPES, pH 7.4 and 290–310 mOsm). The internal solution used was potassium fluoride with ATP (160 mM KF, 2 mM MgCl₂, 10 mM EGTA, 10 mM HEPES, 4 mM NaATP, pH = 7.2 and 300–320 mOsm). A 2-step pulse (applied every 10 sec) from –80 mV first to 40 mV for 2 sec and then to –60 mV for 4 sec, was used to elicit hERG currents. The percent reduction of tail current amplitude by the drugs was determined and data are shown as mean ± SD (n = 3–4 per data point). For all experiments, solutions of

the drugs were prepared fresh from 10 mM stocks in DMSO. The final DMSO concentration never exceeded 1%.

Larval Zebrafish Heart Rate Experiments.

Zebrafish express Zerg, an orthologue of hERG, and many hERG inhibitors induce bradycardia or arrhythmia in zebrafish.³⁵ Heart rate was recorded and calculated as reported previously³⁶ with slight modifications (n = 3–9). Briefly, 7 dpf zebrafish larvae were anesthetized with tricaine (Acros Organics) and immobilized in a lateral orientation using 1% low melt agarose (LMA, Gene Mate) dissolved in egg water.³⁷ Tricaine was washed out and drug was added to 4 mL embryo media in a 6-well plate (final concentration = 50 μ M). Videos were collected at 30 frames per second (fps) using a Leica M80 scope with an ACHRO 1x nosepiece attachment and a Leica IC80 HD camera. Regions of interest (ROIs) were drawn around the atrium and ventricle of individual zebrafish and average pixel dynamics were calculated using the ImageJ plugin Time Series Analyzer V3. This pixel change oscillation was graphically smoothed using the Savgol filter in SciPy. Peaks were detected using the SciPy package “find_peaks”. Peak time interval and BPM were calculated using custom code. The arrhythmia score was calculated as the ratio of atrium BPM to ventricle BPM (n = 6–18).

Larval Zebrafish Behavioral Experiments.

Behavioral data were collected and analyzed as described previously,^{20,22} with slight modifications. Locomotion of 7 dpf zebrafish was recorded at 100 fps under a 17-minute battery of acoustic and light-based stimuli 1 h post-treatment. Data were collected in concentration–response format on eight 96-well plates with 8 zebrafish per well. Each plate contained all 10 compounds at 8 concentrations plus 8 DMSO (vehicle) and 8 eugenol (lethal) control wells. Treatments and well positions were scrambled according to 2 randomized plate layouts. Motion in Extended Data 3a was smoothed using the mean over a 10-frame sliding window. Classifiers were trained as described.²² For Extended Data 3d, 6 repeat vs-solvent and 6 repeat vs-lethal classifiers (3,000 trees) were trained per comparison, each to classify 8 treatment wells and 8 randomly subsampled control wells. Responses were calculated from the out-of-bag (oob) accuracy values as $r = (a-0.4)/(1-0.4)$. 95% confidence intervals were calculated over 1,000 bootstrap samples per comparison. For Extended Data 3b, a single classifier (10,000 trees) was trained on all data for the treatments shown, and the oob predictions were used.

Larval Zebrafish Seizure Experiments.

At 6 dpf, transgenic zebrafish larvae (*Tg(elavl3:GCaMP5G)a4598*)³⁸ were anesthetized with tricaine and immobilized in a dorsal orientation using 1% LMA dissolved in egg water. Tricaine was washed out and zebrafish were treated for 1 h with compounds (50 μ M for IBO and TBG; 15 mM for PTZ). Videos were acquired using a Zeiss Axiozoom.V16, and GCaMP5G fluorescence was induced using a Lumencor sola light engine. Zen software V2 blue edition controlled an AxioCam 506 mono camera set to 33 fps. Short videos (1–3 min) were acquired per condition. Change in fluorescence intensity was calculated using ImageJ from an ROI drawn in the cerebellar region, and F/F was calculated and visualized using custom functions.

Larval Zebrafish Toxicity.

Tropical 5D wild-type larval zebrafish were obtained from the Sinnhuber Aquatic Research Laboratory (SARL) at Oregon State University (Corvallis, Oregon), and subsequent generations were raised at UC Davis. Zebrafish husbandry, spawning, dechoriation of embryos, and exposures were performed as described previously.²⁴ Chemical stocks were prepared at 100 mM in DMSO and diluted to 200 μ M with embryo media. This solution was diluted 2-fold into individual wells of 96-well plates housing larval zebrafish. The final compound and DMSO concentrations were 100 μ M and 0.1% (v/v), respectively. Wells were covered with Parafilm M (Bemis, North America, Neenah, Wisconsin) then covered with the plate lid. Plates were maintained in an incubator at 28.5 °C with a 14 h light (~300 lux)/10 h dark cycle. Fish were statically exposed to compounds 6 h post-fertilization (hpf) through 5 dpf. All compounds were tested for mortality/teratology in triplicate experiments (three experiments conducted on independent days using fish from independent spawns). For each experiment, 16 fish were tested per concentration per compound (n = 48 fish/condition). At 1, 2, 3, 4, and 5 dpf, fish were examined for mortality and developmental malformations using a Leica Stereo Microscope Model S6D (Leica, Germany) up to 4.5x magnification.

Serotonin and Opioid Receptor Functional Assays.

Functional assay screens at 5-HT and opioid receptors were performed in parallel using the same compound dilutions and 384-well format high-throughput assay platforms. Assays assessed activity at all human isoforms of the receptors, except where noted for the mouse 5-HT_{2A} receptor. Receptor constructs in pcDNA vectors were generated from the Presto-Tango GPCR library³⁹ with minor modifications. All compounds were serially diluted in drug buffer (HBSS, 20 mM HEPES, pH 7.4 supplemented with 0.1% bovine serum albumin and 0.01% ascorbic acid) and dispensed into 384-well assay plates using a FLIPR^{TETRA} (Molecular Devices). Every plate included a positive control such as 5-HT (for all 5-HT receptors), DADLE (DOR), salvinorin A (KOR), and DAMGO (MOR). For measurements of 5-HT_{2A}, 5-HT_{2B}, and 5-HT_{2C} Gq-mediated calcium flux function, HEK Flp-In 293 T-Rex stable cell lines (Invitrogen) were loaded with Fluo-4 dye for one hour, stimulated with compounds and read for baseline (0–10 seconds) and peak fold-over-basal fluorescence (5 min) at 25°C on the FLIPR^{TETRA}. For measurement of 5-HT₆ and 5-HT_{7a} functional assays, Gs-mediated cAMP accumulation was detected using the split-luciferase GloSensor assay in HEKT cells measuring luminescence on a Microbeta Trilux (Perkin Elmer) with a 15 min drug incubation at 25°C. For 5-HT_{1A}, 5-HT_{1B}, 5-HT_{1F}, MOR, KOR, and DOR functional assays, Gi/o-mediated cAMP inhibition was measured using the split-luciferase GloSensor assay in HEKT cells, conducted similarly as above, but in combination with either 0.3 μ M isoproterenol (5-HT_{1A}, 5-HT_{1B}, 5-HT_{1F}) or 1 μ M forskolin (MOR, KOR, and DOR) to stimulate endogenous cAMP accumulation. For measurement of 5-HT_{1D}, 5-HT_{1E}, 5-HT₄, and 5-HT_{5A} functional assays, β -arrestin2 recruitment was measured by the Tango assay utilizing HTLA cells expressing TEV fused- β -arrestin2, as described previously³⁹ with minor modifications. Cell lines were not authenticated or tested for mycoplasma contamination. Data for all assays were plotted and non-linear regression was performed using “log(agonist) vs. response” in Graphpad Prism to yield E_{max} and EC₅₀ parameter estimates.

Safety Pharmacology Profiling Panel.

Eurofins Discovery (Taipei, Taiwan) screened TBG (10 μ M) against their SafetyScreen87™ Panel and in their VMAT (Non-Selective) Human Vesicular Monoamine Transporter Binding Assay.

Conditioned Place Preference (CPP).

The CPP apparatus consisted of two chambers (18 cm L x 20 cm W x 35 cm H) connected by a corridor (10 cm L x 20 cm W x 35 cm H). One chamber had a smooth floor and black walls while the second chamber had a mesh floor and patterned walls. A block was placed in the corridor to restrict mice to a particular chamber. On Day 1 (pre-conditioning), male C57/BL6J mice (9–10 weeks old) were allowed to explore the entire apparatus for 30 min. Mice were randomly sorted into treatment groups (TBG at 50 mg/kg, 10 mg/kg and 1 mg/kg), ensuring that their initial preferences for what would become the TBG-paired side were approximately equal. Next, the mice were administered an intraperitoneal injection of either VEH (saline) or TBG (counterbalanced) immediately before being confined to one of the two chambers for 30 min. The following day, the other treatment was administered, and the mice were confined to the opposite chamber for 30 min. This sequence was repeated twice, such that all mice received 3 VEH-side pairings and 3 TBG-side pairings. The mice were returned to their home cages in between treatment-side pairings. On Day 8 (post conditioning), the mice were allowed to explore the entire apparatus for 30 min, and the time spent on the VEH- and TBG-paired sides was quantified using ANYmaze software (version 6.2). The apparatus was cleaned with 70% ethanol between trials. Drug solutions were prepared fresh daily.

Pharmacokinetic Studies.

Male and female C57/BL6J mice (12 weeks old) were administered TBG via intraperitoneal injection at doses of either 50 mg/kg, 10 mg/kg or 1 mg/kg. Mice were sacrificed 15 min or 3 h post-injection via cervical dislocation. Two males and two females were used per dose/timepoint. Brain and liver were harvested, flash frozen in liquid nitrogen, and stored at -80°C until metabolomic processing. Metabolites were extracted from tissue as described previously.⁴⁰ Briefly, whole brain and liver sections were lyophilized overnight to complete dryness, then homogenized with 3.2 mm diameter stainless steel beads using a GenoGrinder for 50 seconds at 1500 rpm. Ground tissue was then extracted using 225 μ L cold methanol, 190 μ L water, 750 μ L methyl tert-butyl ether (MTBE). Seven method blanks and seven quality control (QC) samples (pooled human serum, BioIVT) were extracted at the same time as the samples. The nonpolar fraction of MTBE was dried under vacuum and reconstituted in 60 μ L of 90:10 (v/v) methanol: toluene containing 1-cyclohexyl-dodecanoic acid urea (CUDA) as an internal standard. Samples were then vortexed, sonicated and centrifuged prior to analysis. For analysis of TBG in liver and brain, samples were randomized prior to injection with method blanks and QC samples analyzed between every ten study samples. A six-point calibration curve was analyzed after column equilibration using blank injections, and then after all study samples. Blanks were injected following the calibration curve to ensure no tabernanthalog was retained on the column and carried over to samples. Reconstituted sample (5 μ L) was injected onto a Waters Acquity UPLC CSH C18

column (100 mm x 2.1 mm, 1.7 μ m particle size) with an Acquity UPLC CSH C18 VanGuard precolumn (Waters, Milford, MA) using a Vanquish UHPLC coupled to a TSQ Altis triple quadrupole mass spectrometer (ThermoFisher Scientific, San Jose, CA). Mobile phase A consisted of 60:40 v/v acetonitrile/water with 10 mM ammonium formate and 0.1% formic acid. Mobile phase B was 90:10 v/v isopropanol/acetonitrile with 10 mM ammonium formate and 0.1% formic acid. Gradients were run from 0–2 minutes at 15% B; 2–2.5 minutes 30% B; 2.5–4.5 minutes 48% B; 4.5–7.3 minutes 99% B; 7.3–10 minutes 15% B. The flow rate was 0.600 mL/min and the column was heated to 65°C. Mass spectrometer conditions were optimized for TBG by direct infusion. Selected reaction monitoring for the top five ions, with collision energy, source fragmentation, and radio frequency optimized for TBG. Data were processed with TraceFinder 4.1 (ThermoFisher Scientific, San Jose, CA). Organ weights were recorded. The concentration in the brain was calculated using the experimentally determined number of mols of TBG in the whole organ divided by the weight of the organ.

Spinogenesis Experiments.

Spinogenesis experiments were performed as previously described¹⁴ with the exception that cells were treated on DIV19 and fixed 24 h after treatment on DIV20. The images were taken on a Nikon HCA Confocal microscope with a 100x/NA 1.45 oil objective. DMSO and ketamine (10 μ M) were used as vehicle and positive controls, respectively.

In Vivo Spine Dynamics.

Male and female *Thy1-GFP-M* line mice⁴¹ (n = 5 per condition) were purchased from The Jackson Laboratory (JAX #007788) and maintained in UCSC animal facilities according to an IACUC approved protocol. In vivo transcranial two-photon imaging and data analysis were performed as previously described.⁴² Briefly, mice were anesthetized with an intraperitoneal (i.p.) injection of a mixture of ketamine (87 mg/kg) and xylazine (8.7 mg/kg). A small region of the exposed skull was manually thinned down to 20–30 μ m for optical access. Spines on apical dendrites in mouse primary sensory cortices were imaged using a Bruker Ultima IV two-photon microscope equipped with an Olympus water-immersion objective (40x, NA = 0.8) and a Ti:Sapphire laser (Spectra-Physics Mai Tai, excitation wavelength 920 nm). Images were taken at a zoom of 4.0 (pixel size 0.143 \times 0.143 μ m) and Z-step size of 0.7 μ m. The mice received an i.p. injection of DOI (10 mg/kg) or TBG (50 mg/kg) immediately after they recovered from the anesthesia of the first imaging session. The mice were re-imaged 24 h after drug administration. Dendritic spine dynamics were analyzed using ImageJ. Spine formation and elimination were quantified as percentages of spine numbers on day 0.

Antidepressant-Like Response Following Unpredictable Mild Stress (UMS).

Male and female mice (8 weeks old) were subjected to 7 d of UMS, as described previously.⁴³ Briefly, the following stressors were utilized: Day 1: Light Phase = 30 min of restraint stress x 2; Dark Phase = home cage space reduction. Day 2: Light Phase = exposure to a new room + 30 min on the orbital shaker, sudden loud noise x 5, tail suspension for 6 min; Dark Phase = wet bedding. Day 3: Light Phase = exposure to new mice; Dark Phase = exposure to light. Day 4: Light Phase = social isolation; Dark Phase = tilted cage. Day 5: Light Phase =

tilted cage, island isolation; Dark Phase = no bedding. Day 6: Light Phase = no bedding, random puff of air x 5–10; Dark Phase = foreign objects. Day 7: Light Phase = foreign objects, food deprivation; Dark Phase = food deprivation, continual exposure to loud music. Immediately following UMS, TBG or VEH were administered via intraperitoneal injection, and 24 h later the mice were subjected to a FST using the same procedure as described below.

Forced Swim Test (FST) in the Absence of UMS.

Male C57/BL6J mice (9–10 weeks old at time of experiment) were obtained from the Jackson Lab and housed 4–5 mice/cage in a UCD vivarium following an IACUC approved protocol. After 1 week in the vivarium each mouse was handled for approximately 1 minute by a male experimenter for 3 consecutive days leading up to the first FST. All experiments were carried out by the same male experimenter who performed handling. During the FST, mice underwent a 6 min swim session in a clear Plexiglas cylinder 40 cm tall, 20 cm in diameter, and filled with 30 cm of $24 \pm 1^\circ\text{C}$ water. Fresh water was used for every mouse. After handling and habituation to the experimenter, drug-naïve mice first underwent a pretest swim to more reliably induce a depressive phenotype in the subsequent FST sessions. Immobility scores for all mice were determined after the pre-test and mice were randomly assigned to treatment groups to generate groups with similar average immobility scores to be used for the following two FST sessions. The next day, the mice received intraperitoneal injections of TBG (50 mg/kg), a positive control (ketamine, 3 mg/kg), or vehicle (saline). One additional group received ketanserin (4 mg/kg i.p.) 10 min prior to intraperitoneal administration of TBG (50 mg/kg). The following day, the mice were subjected to the FST and then returned to their home cages. One week later, the FST was performed again to assess the sustained effects of the drugs. All FSTs were performed between the hours of 8 am and 1 pm. Experiments were video-recorded and manually scored offline. Immobility time—defined as passive floating or remaining motionless with no activity other than that needed to keep the mouse's head above water—was scored for the last 4 min of the 6 min trial.

Alcohol Consumption.

Male C57/BL6J mice (6–8 weeks old) were obtained from The Jackson Laboratory (Bar Harbor, ME) and were individually housed in a reverse light/dark cycle room (lights on 10:00pm–10:00am). Temperature was kept constant at $22 \pm 2^\circ\text{C}$, and relative humidity was maintained at $50 \pm 5\%$. Mice were given access to food and tap water *ad libitum*. After one week of habituation to the vivarium, the two-bottle choice alcohol-drinking experiment was conducted as described previously.²⁹ For 7 weeks, mice were given intermittent access in their home cage to alcohol. On Mondays, Wednesdays, and Fridays, two bottles were made available for 24 h—one containing 20% ethanol and another containing only water. On Tuesdays, Thursdays, Saturdays, and Sundays, the mice were only given access to water. After 7 weeks, mice were administered TBG (50 mg/kg) or vehicle (saline) via intraperitoneal injection 3 h before the beginning of a drinking session. Ethanol (g/kg) and water (ml/kg) intake were monitored during the first 4 h (initial binge), the first 24 h, and the second 24 h. Next, the mice were only given water for 48 h before the start of another drinking session when ethanol and water consumption was monitored. The placement (right

or left) of the bottles was altered in each session to control for side preference. Spillage was monitored using an additional bottle in a nearby unused cage. Alcohol preference was calculated as the ratio between alcohol/(water + alcohol). Mice were tested using a counterbalanced, within subject design with one week of drug-free alcohol drinking regimen between treatments. One mouse was excluded because the bottle was leaking.

Sucrose Preference.

Male C57/BL6J mice were individually housed and subjected to a two-bottle choice experiment. First, mice were administered TBG (50 mg/kg) or vehicle (saline) via intraperitoneal injection 3 h before the beginning of a two-bottle choice session. During this 3 h period, mice were not given access to water in an attempt to increase their thirst. At the start of the experiment, mice were given one bottle of water and one bottle of water containing 5% sucrose. Sucrose solution and water intake were monitored during the first 4 h and the first 24 h. Sucrose preference was calculated as the amount of sucrose solution consumed minus the amount of water consumed, divided by the total amount of liquid consumed.

Heroin Self-Administration Behavior.

Subjects were age-matched male (n = 16) and female (n = 16) Wistar rats (Charles River). Rats were single housed in a temperature and humidity-controlled room with a 12 h light/dark cycle (7:00 A.M. lights on) with free access to standard laboratory chow and water. Two rats (one male and one female) were excluded from the final dataset due to defective catheters for a final n = 30 rats. Rats were surgically implanted with an intravenous catheter as previously described.⁴⁴ Heroin self-administration training began at least one week after surgery on a fixed ratio 1 (FR1) schedule of reinforcement. Operant chambers were equipped with both an active (heroin-delivering) and inactive lever, and each heroin infusion (0.04 mg, 50 μ l, 2.85 s) was coupled with delivery of a light cue located above the active lever and a 3.5 kHz tone (5 s). Both levers retracted upon initiation of a heroin infusion and remained retracted during the tone + light heroin cue presentation. After six self-administration sessions (2.5 h) on FR1, rats progressed to a variable ratio 5 (VR5) for three sessions and continued to the final variable ratio 15 (VR15) for five sessions. Rats then began extinction training. Extinction training sessions (1 h) were conducted in the same operant chambers (context) where rats previously self-administered heroin, but in the absence of heroin and its tone + light cue. Both levers remained extended throughout the session, and responding was recorded, but produced no consequence. After completing a total of 7 extinction sessions, rats underwent a cued reinstatement test (1 h, withdrawal day 10–12). During the cue test, the heroin tone + light cues were available, but heroin was not. The first active lever press resulted in presentation of the heroin cues, and then cues were available on a VR5 schedule (active lever only) for the remainder of the test. Lever retraction occurred during cue presentation (as during self-administration). Injections of TBG (40 mg/kg i.p.) or vehicle (VEH) were administered on the third VR15 session, the first extinction session, and the cued reinstatement test. For each of these timepoints, TBG or VEH was injected 30 min prior to placement in the chamber. Treatment groups were balanced based on response rates, heroin intake, and sex. Behavioral sessions were conducted daily (weekdays only). Catheters were flushed after each self-administration

session with cefazolin and taurolidine citrate solution to prevent infection and/or catheter occlusion. Statistical tests were performed in Prism (GraphPad Prism, RRID:SCR_002798; V8.0) software.

Sucrose Self-Administration Behavior.

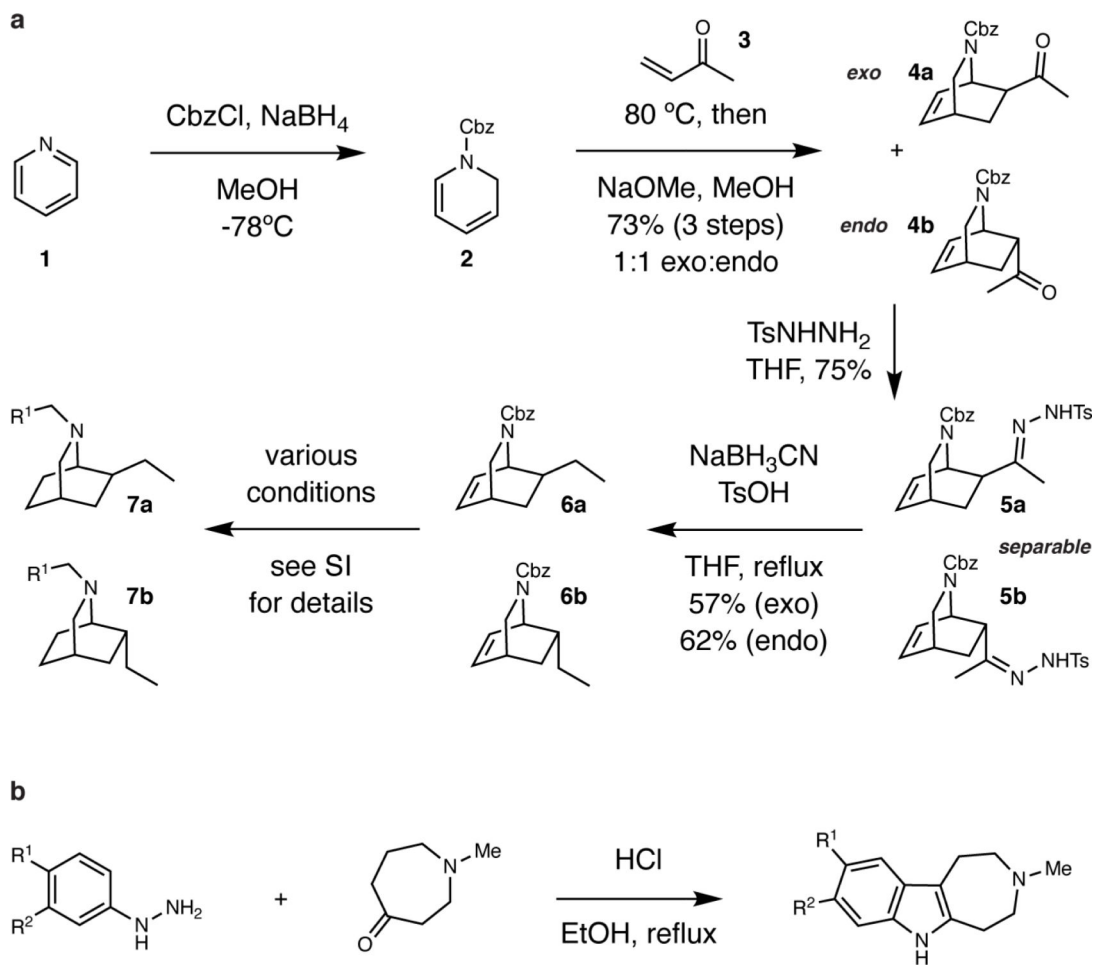
Sucrose self-administration procedures were designed to mimic heroin self-administration conditions. Subjects were age-matched male ($n = 24$) and female ($n = 24$) Wistar rats (Charles River). Rats were single housed and had free access to standard laboratory chow and water throughout the experiment. Eight rats (seven males and one female) were excluded from the final dataset due to failure to acquire sucrose self-administration for a final $n = 40$ rats. The final groups consisted of VEH, SA (2.5), SA (10), SA (40), Ext (40), and CUE (40). The number of animals in each group was 7, 6, 7, 7, 7, 6, respectively (40 animals total). At least one week after arrival and acclimation to the animal facility, sucrose self-administration training began on a fixed ratio 1 (FR1) schedule of reinforcement. Operant chambers were equipped with an active (sucrose-delivering) and inactive lever, and each sucrose reward (45 mg pellet; Bio-Serv F0023) was coupled with the same tone + light cues used for the heroin study. Levers retracted upon pellet delivery and remained retracted during cue presentation (5 s). After six self-administration sessions (2 h) on FR1, rats progressed to a variable ratio 5 (VR5) for three sessions and continued to the final variable ratio 15 (VR15) for five sessions. Rats then began extinction training. Extinction training sessions (1 h) were conducted in the same operant chambers (context) where animals previously self-administered sucrose, but neither sucrose nor the sucrose cues were available. Responding on both levers was recorded during each session, but produced no consequence. After completing 7 extinction sessions, rats underwent a cued reinstatement test (1 h). During the cue test, the sucrose tone + light cues were available, but sucrose was not. The first active lever press resulted in presentation of the sucrose cues, and then cues were available on a VR5 schedule (active lever only) for the remainder of the test. Lever retraction occurred during cue presentation (as during self-administration). Injections were administered on the third VR15 session, the first extinction session, and the cued reinstatement test. For each of these tests, TBG (2.5 mg/kg, 10 mg/kg, or 40 mg/kg IP) or vehicle (VEH) was injected 30 min prior to placement in the chamber. The low (2.5 mg/kg) and intermediate (10 mg/kg) doses of TBG were tested only on the third VR15 sucrose self-administration session. The high dose (40 mg/kg) was tested at all three test time points. Statistical tests were performed in Prism (GraphPad Prism, RRID:SCR_002798; V8.0) software.

Open Field Test.

Naïve male ($n = 7$) and female ($n = 6$) Wistar rats (Charles River) were allowed to acclimate to the animal facility for at least one week after arrival. Spontaneous locomotion in response to a novel open field (44 cm long x 36 cm wide x 43 cm tall) was assessed 30 min after injection of vehicle or TBG (40 mg/kg, i.p.). Videos were recorded with an overhead camera connected to the tracking software EthoVision XT (Noldus, The Netherlands) for subsequent offline analysis. Rats were allowed to move freely in the open field for 30 min, then they were briefly removed from the apparatus to receive an injection of cocaine (15 mg/kg, i.p.). The rats were immediately returned to the open field for an additional hour to assess

cocaine-induced locomotion. Each open field chamber was cleaned with Clidox-S in between sessions. Locomotion was tracked using EthoVision XT to assess the velocity (cm/s) and total distance traveled (m) during the baseline (first 30 min) and cocaine (last 60 min) phases separately. Thigmotaxis was assessed as the percentage of time spent in the center of the apparatus (26 cm long x 18 cm wide; i.e., 9 cm perimeters) was also analyzed during the baseline period to determine if TBG alters anxiety in the open field.

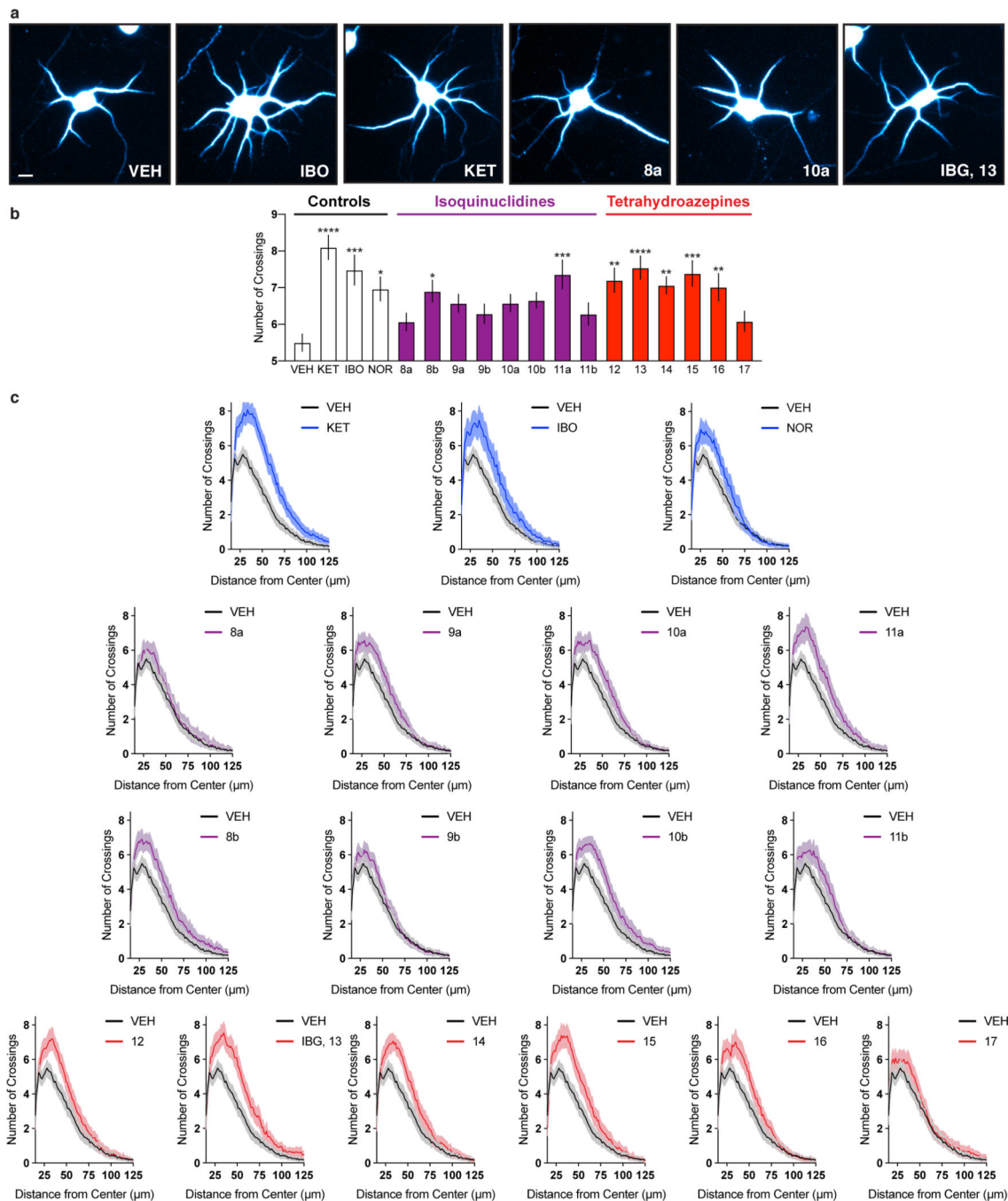
Extended Data



Extended Data Fig. 1. Synthesis of ibogalogs.

(a) Ibogalogs lacking the tetrahydroazepine of ibogaine were synthesized in only a few steps. Briefly, acylation of pyridine **1** under reductive conditions yielded the Cbz-protected dihydropyridine **2**, which was immediately subjected to a Diels-Alder reaction with methyl vinyl ketone (**3**) followed by an in situ epimerization with NaOMe to afford an inseparable 1:1 mixture of *exo* (**4a**) and *endo* (**4b**) isomers (73% over 3 steps). Reaction of **4a** and **4b** with tosylhydrazide yielded the hydrazones **5a** and **5b**, which were separable via a combination of selective crystallization and chromatography (total yield of the two isomers = 75%). Caglioti reduction of the tosylhydrazones yielded **6a** or **6b**, which were readily converted to a variety of analogs via reaction sequences involving hydrogenolysis of the Cbz

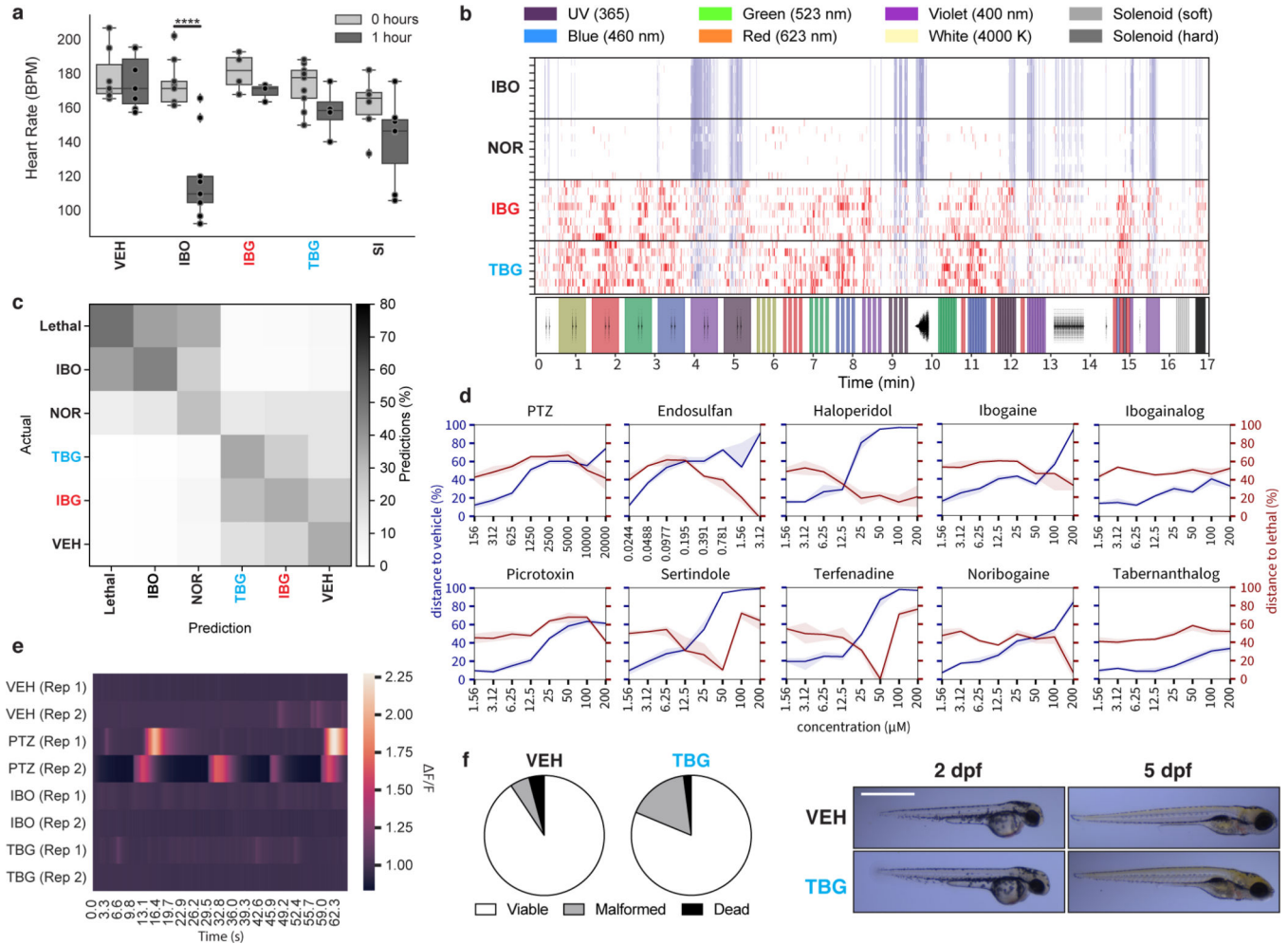
group, hydrogenation of the olefin, and C–N bond formation (see Supporting Information for details). (b) Ibogalogs lacking the isoquinuclidine of ibogaine were synthesized in a single step through Fischer indole cyclization. See Supporting Information for details.



Extended Data Fig. 2. The effects of ibogalogs on dendritogenesis.

(a) Representative images of rat embryonic cortical neurons (DIV6) treated with compounds. Scale bar = 10 μm . (b) Maximum numbers of crossings (N_{max}) of the Sholl plots demonstrate that tetrahydroazepine-containing ibogalogs are more effective at

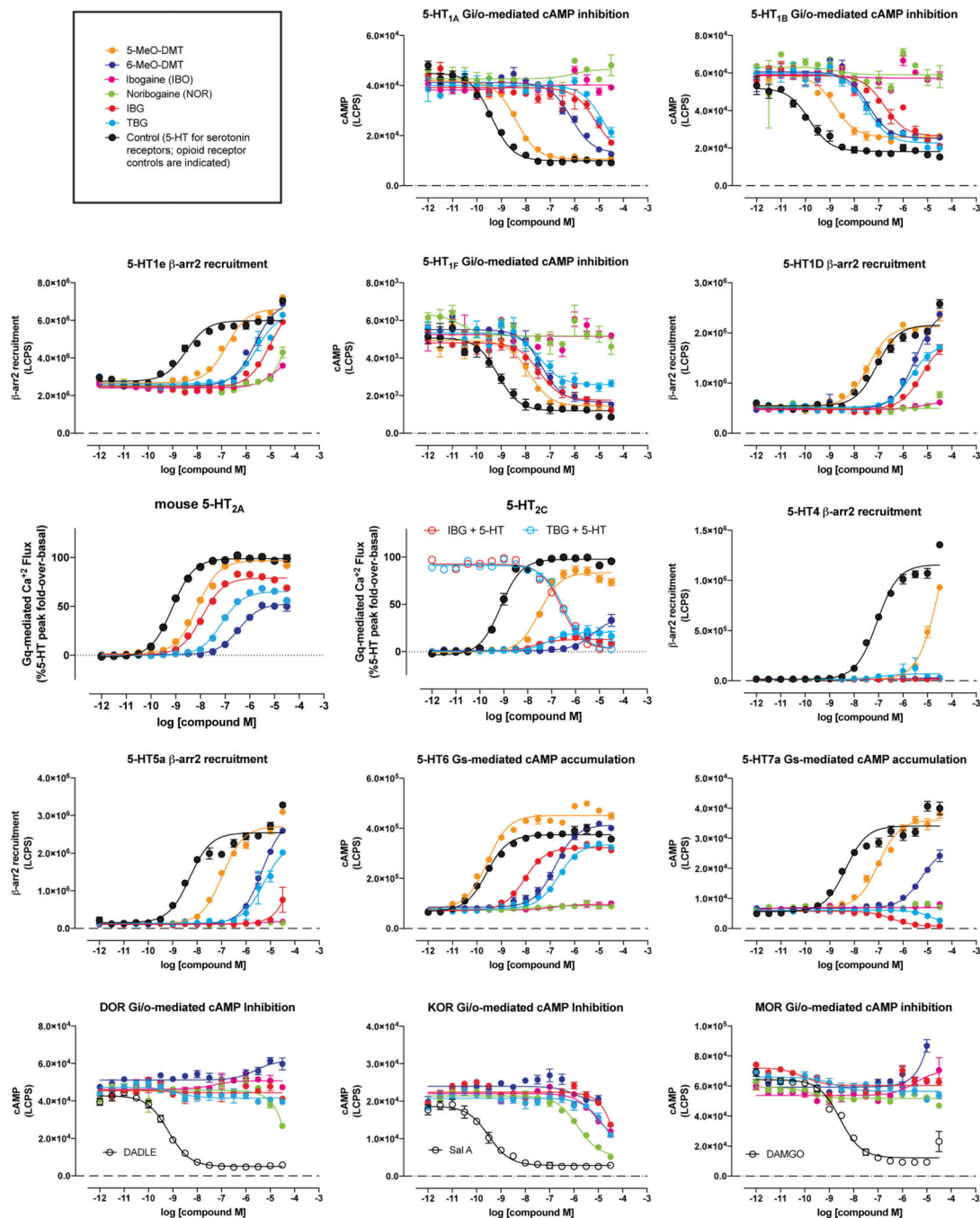
increasing dendritic arbor complexity than are isoquinuclidine-containing ibogalogs. (c) Sholl analysis (circle radii = 1.34 μm increments) demonstrates that cultured cortical neurons treated with several ibogalogs have more complex dendritic arbors as compared to vehicle control (n = 52–83 neurons per treatment). The shaded area surrounding each line represents 95% confidence intervals. Control compounds, isoquinuclidines, and tetrahydrozepines are shown in blue, purple, and red, respectively. Exact N numbers for each experimental condition are reported in Supplementary Table 1. Specific statistical tests, information on reproducibility, and exact p values are reported in the Methods and Supplementary Table 1.



Extended Data Fig. 3. TBG is safer than ibogaine.

(a) Unlike ibogaine, IBG and TBG do not induce bradycardia in larval zebrafish. Sertindole (SI) was used as a positive control. (b) Heatmaps are shown representing aggregate larval zebrafish locomotor activity per well compared to vehicle controls (pseudo-Z-score). Red and blue indicate higher and lower activity than the mean of vehicle controls, respectively, while white indicates activity within ± 1 SD from control. Stimuli applied over time are indicated under the heatmaps. Colors indicate bright LED light of respective colors, black traces represent the waveforms of acoustic stimuli, and gray vertical lines indicate physical

tapping as secondary acoustic stimuli. (c) Confusion matrix for classification of compounds (200 μM) plus VEH and lethal controls. (d) Concentration–response curves are shown for treated zebrafish subjected to the battery of stimuli depicted in Extended Data 3b. Lower percentages indicate treatments that were more often classified as vehicle (blue) or lethal (red). The solid line denotes the median and the shading denotes a 95th percentile confidence interval calculated by bootstrap. $N = 8$ wells / condition (64 zebrafish / condition). Blue lines indicate that all compounds produce behavioral phenotypes more distinct from vehicle at higher concentrations. Red lines indicate that known toxins (e.g., PTZ, picrotoxin, endosulfan), known hERG inhibitors (sertindole, haloperidol, terfenadine), and iboga alkaloids (IBO, NOR) produce behavioral phenotypes more closely resembling a lethal phenotype as their concentrations are increased. Increasing concentrations of IBG or TBG do not produce lethal-like behavioral phenotypes. (e) Transgenic larval zebrafish expressing GCaMP5G were immobilized in agarose, treated with compounds, and imaged over time. The known seizure-inducing compound PTZ was used as a positive control. Ibogaine and TBG were treated at 50 μM ($n = 2$ per condition). (f) Proportion of viable and non-viable (malformed + dead) zebrafish following treatment with VEH and TBG (66 μM) for 5 dpf (Fisher's exact test: $p = 0.3864$). Representative images of zebrafish treated with VEH and TBG (66 μM) for 2 and 5 dpf are shown. Scale bar = 2 mm. Exact N numbers for each experimental condition are reported in Supplementary Table 1. Specific statistical tests, information on reproducibility, and exact p values are reported in the Methods and Supplementary Table 1.

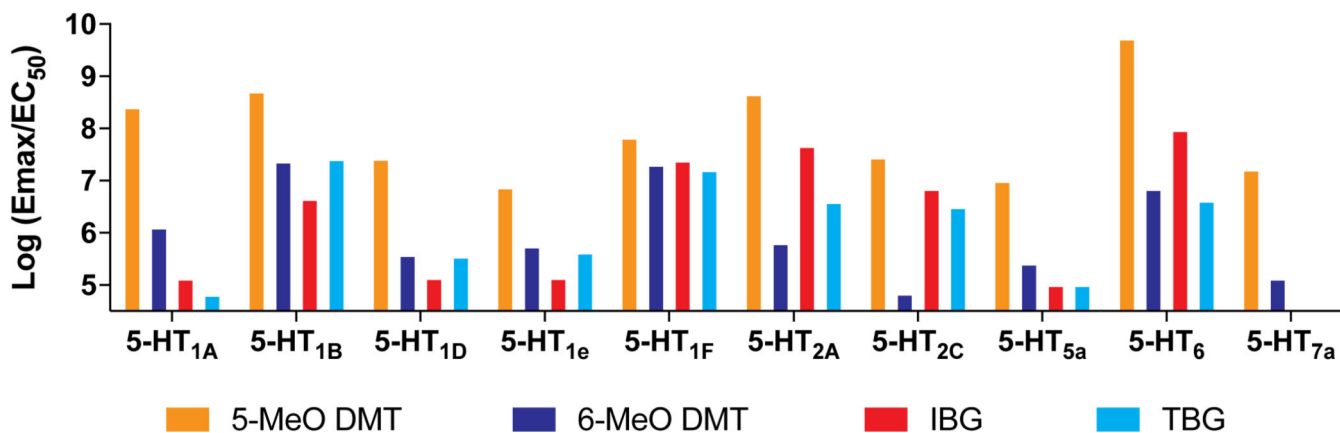


Extended Data Fig. 4. Concentration-response curves demonstrating the abilities of ibogalogs and related compounds to activate 5-HT and opioid receptors.

All compounds were assayed in parallel using the same drug dilutions. Graphs reflect representative concentration-response curves plotting mean and SEM of data points performed in duplicate or triplicate. Assay details are described in the methods. Exact N numbers for each experimental condition are reported in Supplementary Table 1. Specific statistical tests, information on reproducibility, and exact p values are reported in the Methods and Supplementary Table 1.

Target Receptor	5-MeO-DMT			6-MeO-DMT			IBG			TBG			IBO			NOR		
	EC ₅₀ , nM	E _{max} % Control	log(E _{max} /EC ₅₀)	EC ₅₀ , nM	E _{max} % Control	log(E _{max} /EC ₅₀)	EC ₅₀ , nM	E _{max} % Control	log(E _{max} /EC ₅₀)	EC ₅₀ , nM	E _{max} % Control	log(E _{max} /EC ₅₀)	EC ₅₀ , nM	E _{max} % Control	log(E _{max} /EC ₅₀)	EC ₅₀ , nM	E _{max} % Control	log(E _{max} /EC ₅₀)
5-HT1A	3.92	98	8.40	725.40	91	6.10	6911.00	91	5.12	14600.0	95	4.81	Inactive	Inactive	Inactive	Inactive	Inactive	Inactive
5-HT1B	1.53	78	8.71	37.06	85	7.36	170.40	76	6.65	33.66	87	7.41	Inactive	Inactive	Inactive	Inactive	Inactive	Inactive
5-HT1D	37.01	98	7.42	3246.00	120	5.57	6043.00	82	5.13	2180.00	76	5.54	Inactive	Inactive	Inactive	Inactive	Inactive	Inactive
5-HT1e	160.20	119	6.87	2363.00	131	5.74	9309.00	126	5.13	2784.00	117	5.62	Inactive	Inactive	Inactive	Inactive	Inactive	Inactive
5-HT1F	14.00	93	7.82	44.50	88	7.30	35.10	85	7.38	40.40	64	7.20	Inactive	Inactive	Inactive	Inactive	Inactive	Inactive
5-HT2A	1.85	82	8.65	1003.00	63	5.80	18.10	82	7.66	147.00	57	6.59	Inactive	Inactive	Inactive	Inactive	Inactive	Inactive
5-HT2B	5.87	73	8.09	Inactive	Inactive	Inactive	Inactive	Inactive	Inactive	Inactive	Inactive	Inactive	Inactive	Inactive	Inactive	Inactive	Inactive	Inactive
5-HT2C	30.70	84	7.44	5358.00	36	4.83	19.00	13	6.84	68.50	21	6.49	Inactive	Inactive	Inactive	Inactive	Inactive	Inactive
5-HT4	>10,000	N.D.	<5.00	>10,000	N.D.	<5.00	>10,000	N.D.	<5.00	>10,000	N.D.	<5.00	Inactive	Inactive	Inactive	Inactive	Inactive	Inactive
5-HT5a	110.00	107	6.99	4543.00	117	5.41	>10,000	N.D.	<5.00	>10,000	N.D.	<5.00	Inactive	Inactive	Inactive	Inactive	Inactive	Inactive
5-HT6	0.24	125	9.72	162.00	113	6.84	8.80	83	7.97	214.00	87.5	6.61	Inactive	Inactive	Inactive	Inactive	Inactive	Inactive
5-HT7a	65.70	107	7.21	5653.00	75	5.12	335.00	-17	N.D.	>10,000	N.D.	N.D.	N.D.	N.D.	N.D.	N.D.	N.D.	N.D.
MOR	Inactive	Inactive	Inactive	Inactive	Inactive	Inactive	Inactive	Inactive	Inactive	Inactive	Inactive	Inactive	Inactive	Inactive	Inactive	Inactive	Inactive	Inactive
KOR	Inactive	Inactive	Inactive	>10,000	N.D.	<5.00	>10,000	N.D.	<5.00	>10,000	N.D.	<5.00	>10,000	N.D.	<5.00	1400	85	5.78
DOR	Inactive	Inactive	Inactive	Inactive	Inactive	Inactive	Inactive	Inactive	Inactive	Inactive	Inactive	Inactive	Inactive	Inactive	Inactive	Inactive	Inactive	Inactive

5-HT Receptor Activity



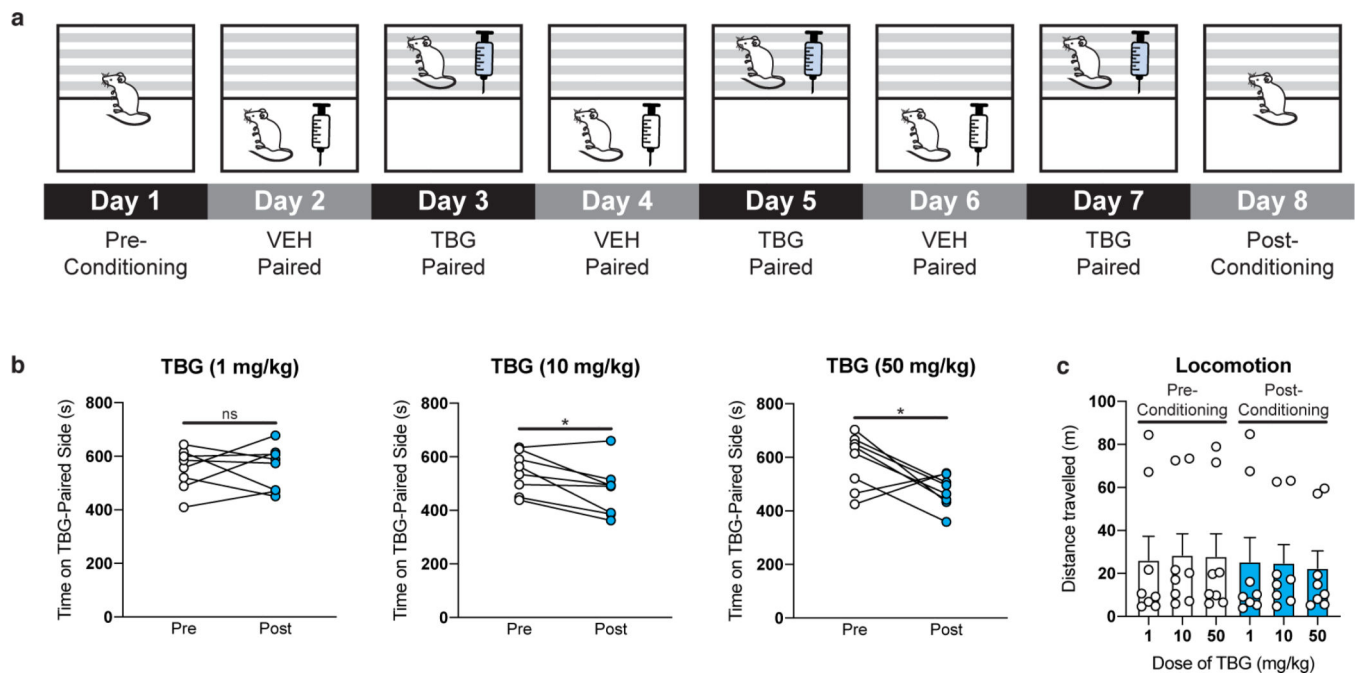
Extended Data Fig. 5. Pharmacological profiles of ibogalogs and related compounds. EC₅₀ and E_{max} estimates from at least two independent concentration-response curves performed in duplicate or triplicate. Log(E_{max}/EC₅₀) activity is included as an estimate of system agonist activity. Inactive = inactive in agonist mode; N.D. = not determined; blue boxes = exhibits antagonist activity; dark grey boxes = inactive in agonist mode but not tested in antagonist mode; orange boxes indicate inverse agonist. Ibogalogs are more selective 5-HT_{2A} agonists than 5-MeO-DMT. Exact N numbers for each experimental condition are reported in Supplementary Table 1. Specific statistical tests, information on reproducibility, and exact p values are reported in the Methods and Supplementary Table 1.

Author Manuscript

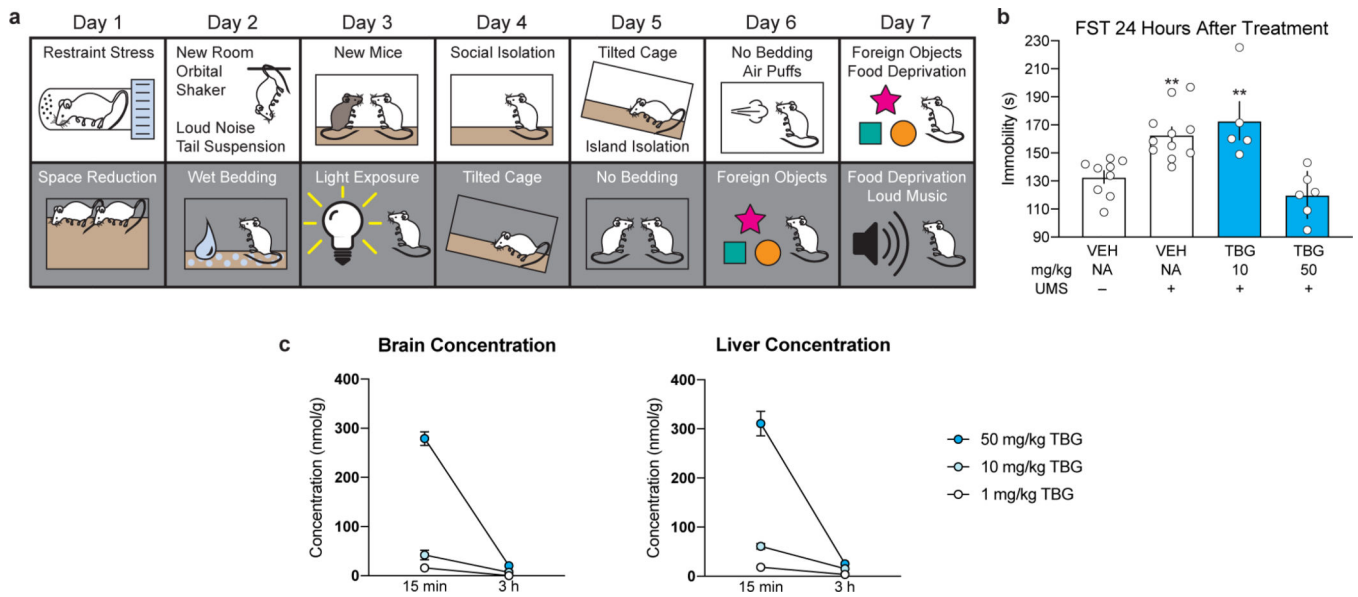
Author Manuscript

Author Manuscript

Author Manuscript

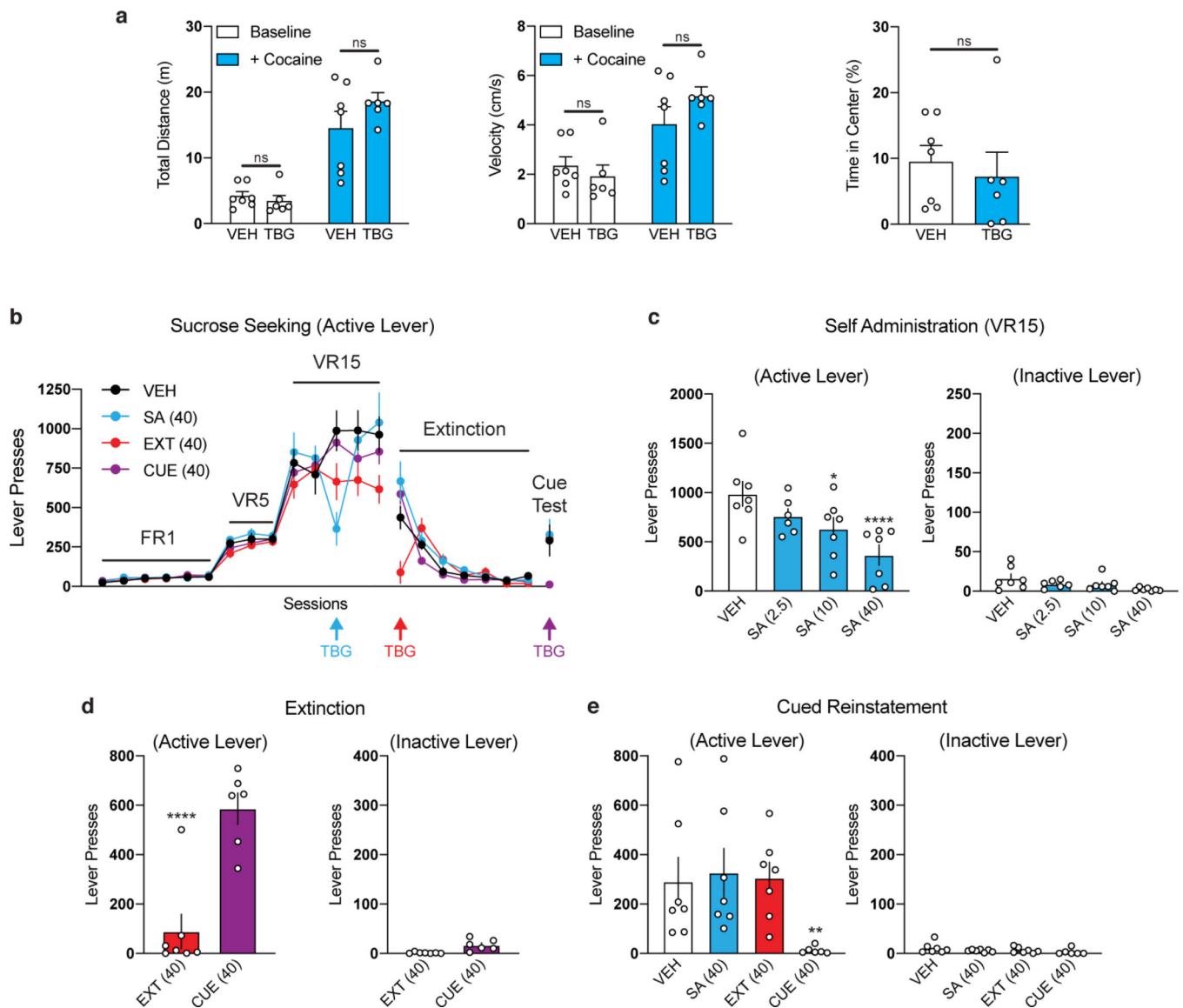


Extended Data Fig. 6. High doses of TBG do not produce a conditioned place preference (CPP). (a) Schematic illustrating the design of the CPP experiments. On day 1, the amount of time the mice spent in each distinct side of a two-chamber apparatus was recorded. Next, VEH and TBG were administered to mice on alternating days while they were confined to chamber A (white box) or B (gray parallel lines), respectively. Conditioning lasted for a total of 6 days. On day 8, preference for each distinct side of the two-chamber apparatus was assessed. (b) A low dose of TBG (1 mg/kg) did not produce CPP or conditioned place aversion (CPA). Higher doses (10 and 50 mg/kg) produce a modest CPA. (c) TBG does not produce any long-lasting (>24 h) effects on locomotion. There is no statistical difference in locomotion between any pre- or post-conditioning groups ($p = 0.9985$, one-way ANOVA). White bars indicate groups prior to receiving TBG (i.e, pre-conditioning), while blue bars indicate groups 24 h after the last TBG administration (i.e, post-conditioning). Exact N numbers for each experimental condition are reported in Supplementary Table 1. Specific statistical tests, information on reproducibility, and exact p values are reported in the Methods and Supplementary Table 1.



Extended Data Fig. 7. TBG produces antidepressant effects in mice.

(a) Schematic illustrating the stressors employed as part of the 7-day UMS protocol. White and grey boxes represent the light and dark phases of the light cycle, respectively. (b) TBG rescues the effects of UMS on immobility. (c) TBG (50 mg/kg) reaches high brain concentrations and is rapidly eliminated from the body. Mice were administered 3 different doses of TBG via intraperitoneal injection and sacrificed either 15 min or 3 h later. Whole brains and livers were collected, dried, homogenized, and extracted with methyl tert-butyl ether. Quantification was accomplished using LC-MS and concentrations of TBG in the two organs were calculated. Several samples for the 10 and 1 mg/kg doses at the 3 h time point had TBG at levels below the limit of quantification (~5 nmol/g). In those cases, the values were recorded as 0. Exact N numbers for each experimental condition are reported in Supplementary Table 1. Specific statistical tests, information on reproducibility, and exact p values are reported in the Methods and Supplementary Table 1.



Extended Data Fig. 8. Effects of TBG on locomotion and sucrose-seeking behavior in rats.

(a) Acute administration of TBG does not impair locomotion in the open field. Rats were subjected to novelty-induced locomotion (Baseline) for 30 min. At that time, cocaine was administered and psychostimulant-induced locomotion (+ Cocaine) was assessed for 60 min. There were no differences between the VEH- and TBG-treated groups with respect to total distance traveled or average velocity. Furthermore, there was no difference in thigmotaxis measured during the baseline period (i.e., % time in the center of the open field). (b–e) A sucrose self-administration experiment was conducted in a similar manner to the heroin self-administration experiment in Fig. 4. Doses in mg/kg are shown in parentheses. (b) Sucrose seeking over time is shown. Colored arrows indicate when each group received TBG. VEH was administered at all other time points to each group. (c) TBG acutely reduces sucrose-seeking behavior in a dose-dependent manner when administered during self-administration. (d) TBG acutely reduces sucrose seeking when administered immediately before the first extinction session. The CUE (injection 1 = VEH, injection 2 = VEH) and EXT (injection 1 =


VEH, injection 2 = TBG) groups were compared, as they were matched for the number of withdrawal days between the last self-administration and first extinction session. (o) TBG does not have long-lasting effects on sucrose-seeking behavior, as it does not reduce active lever pressing during the cued reinstatement when administered 12–14 days prior during self-administration (SA) or immediately before extinction (EXT). Exact N numbers for each experimental condition are reported in Supplementary Table 1. Specific statistical tests, information on reproducibility, and exact p values are reported in the Methods and Supplementary Table 1.







Extended Data Table 1.
TBG and IBG are more soluble than ibogaine.

(a) The fumarate salts of TBG and IBG are readily soluble in saline (0.9%) while ibogaine hydrochloride is not. (b) Ibogaine hydrochloride exhibits limited solubility in various saline-based vehicles. Solutions of saline (0.9%) containing various percentages of co-solvents/additives were added to finely crushed ibogaine hydrochloride. All of our attempts to improve its solubility through pulverizing, sonication, and mild heating (< 50 °C) were unsuccessful. Moreover, the addition of co-solvents (ethanol, dimethyl sulfoxide, glycerol), surfactants (Kolliphor), or hydrotropes (ATP) to the vehicle did not substantially improve its solubility. We confirmed the purity and identity of the ibogaine hydrochloride used in these studies through a combination of NMR, LC-MS, and X-ray crystallography experiments. Exact N numbers for each experimental condition are reported in Supplementary Table 1. Specific statistical tests, information on reproducibility, and exact p values are reported in the Methods and Supplementary Table 1.

a			
Solubility at [Cmpd] (mg/mL)			
Cmpd	40	8	4
IBO	no ×	no ×	no ×
IBG	yes ✓	yes ✓	yes ✓
TBG	yes ✓	yes ✓	yes ✓

b		
Vehicle Conditions	Concentration	Soluble?
Saline + 10% EtOH + 10% DMSO	40 mg/ml	NO



Saline + 10% EtOH	8 mg/ml	NO	
Saline + 10% DMSO	8 mg/ml	NO	
Saline + 10% EtOH + 10% DMSO	8 mg/ml	NO	
Saline + 10% EtOH + 10% Kolliphor	8 mg/ml	NO	
Saline + 10% EtOH + 20% Kolliphor	8 mg/ml	NO	
Saline + 10% EtOH + 25% Kolliphor	8 mg/ml	NO	
Saline + 10% EtOH + 30% Kolliphor	8 mg/ml	NO	

Saline + 10% EtOH + 40% Kolliphor	8 mg/ml	NO	
Saline + 10% DMSO + 10% Kolliphor	8 mg/ml	NO	
Saline + 10% DMSO + 25% Kolliphor	8 mg/ml	NO	
Saline + 10% DMSO + 15% Glycerol	8 mg/ml	NO	
Saline + 10 mM ATP	8 mg/ml	NO	
Saline + 10% DMSO	4 mg/ml	NO	
Saline + 10% DMSO + 25% Kolliphor	4 mg/ml	NO	

Saline + 10% DMSO

1 mg/ml

YES



Extended Data Table 2.
Safety Pharmacology Screen.

The effects of TBG (10 μ M) on a wide range of targets was assessed by Eurofins Discovery. Assays were conducted in duplicate and the results were averaged. Targets with $\geq 50\%$ inhibition are highlighted in blue. Exact N numbers for each experimental condition are reported in Supplementary Table 1. Specific statistical tests, information on reproducibility, and exact p values are reported in the Methods and Supplementary Table 1.

Eurofins Catalog #	Assay Name	Species	% Inhibition
107710	ATPase, Na ⁺ /K ⁺ , Heart, Pig	pig	-9
104010	Cholinesterase, Acetyl, ACES	human	13
116030	Cyclooxygenase COX-1	human	16
118030	Cyclooxygenase COX-2	human	7
140010	Monoamine Oxidase MAO-A	human	66
140120	Monoamine Oxidase MAO-B	human	16
107300	Peptidase, Angiotensin Converting Enzyme	rabbit	2
112510	Peptidase, CTSG (Cathepsin G)	human	-2
152300	Phosphodiesterase PDE3A	human	6
154420	Phosphodiesterase PDE4D2	human	1
200510	Adenosine A1	human	-4
200610	Adenosine A2A	human	-8
203110	Adrenergic α 1A	human	15
203210	Adrenergic α 1B	human	20
203400	Adrenergic α 1D	human	15
203630	Adrenergic α 2A	human	81
203710	Adrenergic α 2B	human	27
204010	Adrenergic β 1	human	9
204110	Adrenergic β 2	human	9
206000	Androgen (Testosterone)	human	6
210030	Angiotensin AT1	human	3
212620	Bradykinin B2	human	9
214510	Calcium Channel L-Type, Benzothiazepine	rat	18
214600	Calcium Channel L-Type, Dihydropyridine	rat	6
215000	Calcium Channel L-Type, Phenylalkylamine	rat	42
216000	Calcium Channel N-Type	rat	-3

Eurofins Catalog #	Assay Name	Species	% Inhibition
217050	Cannabinoid CB1	human	1
217100	Cannabinoid CB2	human	-21
217510	Chemokine CCR1	human	11
244500	Chemokine CXCR2 (IL-8RB)	human	-2
219500	Dopamine D1	human	3
219600	Dopamine D2L	human	18
219700	Dopamine D2S	human	0
224010	Endothelin ETA	human	8
226010	Estrogen ER α	human	1
226810	GABAA, Chloride Channel, TBOB	rat	-1
226600	GABAA, Flunitrazepam, Central	rat	-2
226630	GABAA, Ro-15-1788, Hippocampus	rat	10
228610	GABAB1A	human	0
232030	Glucocorticoid	human	12
232600	Glutamate, AMPA	rat	8
232710	Glutamate, Kainate	rat	8
237000	Glutamate, Metabotropic, mGlu5	human	1
232810	Glutamate, NMDA, Agonism	rat	0
232910	Glutamate, NMDA, Glycine	rat	2
233000	Glutamate, NMDA, Phencyclidine	rat	3
234000	Glutamate, NMDA, Polyamine	rat	-2
239000	Glycine, Strychnine-Sensitive	rat	19
239610	Histamine H1	human	35
239710	Histamine H2	human	-12
250460	Leukotriene, Cysteinyl CysLT1	human	3
251100	Melanocortin MC1	human	-3
251350	Melanocortin MC4	human	-8
252610	Muscarinic M1	human	2
252710	Muscarinic M2	human	13
252810	Muscarinic M3	human	18
252910	Muscarinic M4	human	7
257010	Neuropeptide Y Y1	human	16
258700	Nicotinic Acetylcholine α 1, Bungarotoxin	human	19
258730	Nicotinic Acetylcholine α 3 β 4	human	16
260130	Opiate δ 1 (OP1, DOP)	human	14
260210	Opiate κ (OP2, KOP)	human	7
260410	Opiate μ (OP3, MOP)	human	17
299037	Platelet Activating Factor (PAF)	human	7
265600	Potassium Channel [KATP]	hamster	6
265900	Potassium Channel hERG	human	28
267500	PPAR γ	human	-6
299005	Progesterone PR-B	human	4

Eurofins Catalog #	Assay Name	Species	% Inhibition
271110	Serotonin (5-Hydroxytryptamine) 5-HT1A	human	39
271230	Serotonin (5-Hydroxytryptamine) 5-HT1B	human	66
271650	Serotonin (5-Hydroxytryptamine) 5-HT2A	human	57
271700	Serotonin (5-Hydroxytryptamine) 5-HT2B	human	86
271800	Serotonin (5-Hydroxytryptamine) 5-HT2C	human	99
271910	Serotonin (5-Hydroxytryptamine) 5-HT3	human	14
279510	Sodium Channel, Site 2	rat	24
255520	Tachykinin NK1	human	18
202000	Transporter, Adenosine	guinea pig	-9
226400	Transporter, GABA	rat	1
274030	Transporter, SERT	human	88
287530	Vasopressin V1A	human	-6
252030	Transporter, Vesicular Monoamine (Non-Selective)	human	10

Supplementary Material

Refer to Web version on PubMed Central for supplementary material.

Acknowledgement

This work was supported by funds from the National Institutes of Health (NIH) (R01GM128997 to DEO, R37AA01684 to DR, R01AA022583 to DK, R01MH109475 to YZ, R01MH104227 to YZ, R01NS104950 to YZ, R01DA045836 to JP, and U19AG023122 to OF), a Hellman Fellowship (DEO), UC Davis STAIR and STAIR Plus grants (DEO), a Max Planck Fellowship at MPFI (YZ), four NIH training grants (T32GM113770 to RJT, T32MH112507 to LPC, 5T32GM099608 to MV, and 4T32GM6754714 to DMT), two UC Davis Provost's Undergraduate Fellowships (to JV and AJP), the Paul G. Allen Family Foundation (MM and DK), the Genentech Fellowship Program (DMT), and a Medical College of Wisconsin Research Affairs Counsel Pilot Grant (JDM). BMB was supported by the National Center for Advancing Translational Sciences, National Institutes of Health, through grant number UL1 TR001860 and linked award TL1 TR001861. Delix Therapeutics funded the large receptor screen conducted at Eurofins Discovery. We thank Florence F. Wagner for her help coordinating with Eurofins Discovery. This project used the Biological Analysis Core of the UC Davis MIND Institute Intellectual and Development Disabilities Research Center (U54 HD079125). The Olympus FV1000 confocal used in this study was purchased using NIH Shared Instrumentation Grant 1S10RR019266-01. We thank the MCB Light Microscopy Imaging Facility, which is a UC Davis Campus Core Research Facility, for the use of this microscope. Several of the drugs used in this study were provided by the NIDA Drug Supply Program. We also thank Dennis R. Carty for assistance with larval zebrafish toxicity assays.

Data Availability.

Data are available at the following link <https://doi.org/10.6084/m9.figshare.11634795>.

Abbreviations.

VEH	vehicle
KET	ketamine
IBO	ibogaine
NOR	noribogaine

IBG	ibogainalog
TBG	tabernanthalog
KETSN	ketanserin
SI	sertindole
BPM	beats per minute
DOI	2,5-dimethoxy-4-iodoamphetamine
MDMA	3,4-methylenedioxyamphetamine
DMT	<i>N,N</i> -dimethyltryptamine
FST	forced swim test
EtOH	ethanol
DMSO	dimethyl sulfoxide
ATP	adenosine triphosphate
dpf	days post fertilization
PTZ	pentylentetrazole

REFERENCES

1. Wasco MJ; Witt-Enderby PA; Surratt CK DARK Classics in Chemical Neuroscience: Ibogaine. ACS Chem. Neurosci, 2018, 9, 2475–2483. [PubMed: 30216039]
2. Noller GE; Frampton CM; Yazar-Klosinski B Ibogaine Treatment Outcomes for Opioid Dependence from a Twelve-Month Follow-up Observational Study. Am. J. Drug Alcohol Abuse, 2018, 44, 37–46. [PubMed: 28402682]
3. He DY; McGough NN; Ravindranathan A; Jeanblanc J; Logrip ML; Phamluong K; Janak PH; Ron D Glial cell line-derived neurotrophic factor mediates the desirable actions of the anti-addiction drug ibogaine against alcohol consumption. J. Neurosci, 2005, 25, 619–628. [PubMed: 15659598]
4. Marton S; González B; Rodríguez-Bottero S; Miquel E; Martínez-Palma L; Pazos M; Prieto JP; Rodríguez P; Sames D; Seoane G; Scorza C; Cassina P; Carrera I Ibogaine Administration Modifies GDNF and BDNF Expression in Brain Regions Involved in Mesocorticolimbic and Nigral Dopaminergic Circuits. Front. Pharmacol, 2019, 10, 193. doi: 10.3389/fphar.2019.00193. [PubMed: 30890941]
5. Jenks CW Extraction studies of Tabernanthe iboga and Voacanga africana. Nat. Prod. Lett, 2002, 16, 71–76. [PubMed: 11942686]
6. Iyer RN; Favela D; Zhang G; Olson DE The Iboga Enigma: The Chemistry and Neuropharmacology of Iboga Alkaloids and Related Analogs. Nat. Prod. Rep, 2020, doi: 10.1039/d0np00033g.
7. Hough LB; Pearl SM; Glick SD Tissue Distribution of Ibogaine after Intraperitoneal and Subcutaneous Administration. Life Sci, 1996, 58, 119–122.
8. Koenig X; Kovar M; Boehm S; Sandtner W; Hilber K Anti-Addiction Drug Ibogaine Inhibits HERG Channels: A Cardiac Arrhythmia Risk. Addict. Biol, 2014, 19, 237–239. [PubMed: 22458604]
9. Thurner P; Stary-Weinzinger A; Gafar H; Gawali VS; Kudlacek O; Zezula J; Hilber K; Boehm S; Sandtner W; Koenig X Mechanism of HERG Channel Block by the Psychoactive Indole Alkaloid Ibogaine. J. Pharmacol. Exp. Ther, 2014, 348, 346–358. [PubMed: 24307198]

10. Alper KR; Stajic M; Gill JR Fatalities Temporally Associated with the Ingestion of Ibogaine. *J. Forensic Sci.* 2012, 57, 398–412. [PubMed: 22268458]
11. Koenig X; Hilber K The Anti-Addiction Drug Ibogaine and the Heart: A Delicate Relation. *Molecules*, 2015, 20, 2208– 2228. [PubMed: 25642835]
12. Baumann MH; Pablo JP; Ali SF; Rothman RB; Mash DC Noribogaine (12-Hydroxyibogamine): A Biologically Active Metabolite of the Antiaddictive Drug Ibogaine. *Ann. N. Y. Acad. Sci.* 2000, 914, 354–368. [PubMed: 11085335]
13. Olson DE Psychoplastogens: A Promising Class of Plasticity-Promoting Neurotherapeutics. *J. of Exp. Neurosci.* 2018, 12, 1–4.
14. Ly C; Greb AC; Cameron LP; Wong JM; Barragan EV; Wilson PC; Burbach KF; Soltanzadeh Zarandi S; Sood A; Paddy MR; Duim WC; Dennis MY; McAllister AK; Ori-McKenney KM; Gray JA; Olson DE Psychedelics Promote Structural and Functional Neural Plasticity. *Cell Rep*, 2018, 23, 3170–3182. [PubMed: 29898390]
15. Bogenschutz MP; Johnson MW Classic hallucinogens in the treatment of addictions. *Prog. Neuropsychopharmacol. Biol. Psychiatry*, 2016, 64, 250–258. [PubMed: 25784600]
16. Wender PA; Verma VA; Paxton TJ; Pillow TH Function Oriented Synthesis, Step Economy, and Drug Design. *Acc. Chem. Res.* 2008, 41, 40–49. [PubMed: 18159936]
17. Gassaway MM; Jacques TL; Kruegel AC; Karpowicz RJ Jr.; Li X; Li S; Myer Y; Sames D Deconstructing the Iboga Alkaloid Skeleton: Potentiation of FGF2-induced Glial Cell Line-Derived Neurotrophic Factor Release by a Novel Compound. *ACS Chem. Biol.* 2016, 11, 77–87. [PubMed: 26517751]
18. Wager TT; Hou X; Verhoest PR; Villalobos A Central Nervous System Multiparameter Optimization Desirability: Application in Drug Discovery. *ACS Chem. Neurosci.* 2016, 6, 767–775.
19. Glennon RA; Young R.I.; Jacyno JM; Slusher M; Rosecrans JA DOM-stimulus generalization to LSD and other hallucinogenic indolealkylamines. *Eur. J. Pharmacol.* 1983, 86, 453–459. [PubMed: 6572591]
20. Dunlap LE; Azinfar A; Ly C; Cameron LP; Viswanathan J; Tombari RJ; Myers-Turnbull D; Taylor JC; Grodzki AC; Lein PJ; Kokel D; Olson DE Identification of Psychoplastogenic N,N-Dimethylaminoisotryptamine (isoDMT) Analogs Through Structure-Activity Relationship Studies. *J. Med. Chem.* 2019, 2020, 63, 1142–1155.
21. Halberstadt AL; Chatha M; Klein AK; Wallach J; Brandt SD Correlation between the potency of hallucinogens in the mouse head-twitch response assay and their behavioral and subjective effects in other species. *Neuropharmacology*, 2020, 167, 107933. [PubMed: 31917152]
22. McCarroll MN; Gendele L; Kinser R; Taylor J; Bruni G; Myers-Turnbull D; Hellsell C; Carbajal A; Rinaldi C; Kang HJ; Gong JH; Sello JK; Tomita S; Peterson RT; Keiser MJ; Kokel D Zebrafish Behavioural Profiling Identifies GABA and Serotonin Receptor Ligands Related to Sedation and Paradoxical Excitation. *Nat. Commun.* 2019, 10, 4078. doi: 10.1038/s41467-019-11936-w. [PubMed: 31501447]
23. Breuer L; Kasper BS; Schwarze B; Gschossmann JM; Kornhuber J; Müller HH “Herbal seizures”--atypical symptoms after ibogaine intoxication: a case report. *J. Med. Case Rep.* 2015, 9, 243. [PubMed: 26518760]
24. Dach K; Yaghoobi B; Schmuck MR; Carty DR; Morales KM; Lein PJ Teratological and Behavioral Screening of the National Toxicology Program 91-Compound Library in Zebrafish (*Danio rerio*). *Toxicol. Sci.* 2019, 167, 77–91. [PubMed: 30364989]
25. Rothman RB; Baumann MH Serotonergic drugs and valvular heart disease. *Expert Opin. Drug Saf.* 2009, 8, 317–329. [PubMed: 19505264]
26. Phoumthippavong V; Barthas F; Hassett S; Kwan AC Longitudinal Effects of Ketamine on Dendritic Architecture In Vivo in the Mouse Medial Frontal Cortex. *eNeuro*, 2016, 3, pii: ENEURO.0133–15.2016. doi: 10.1523/ENEURO.0133-15.2016.
27. Moda-Sava RN; Murdock MH; Parekh PK; Fetcho RN; Huang BS; Huynh TN; Witzum J; Shaver DC; Rosenthal DL; Always EJ; Lopez K; Meng Y; Nellissen L; Grosenick L; Milner TA; Deisseroth K; Bito H; Kasai H; Liston C Sustained rescue of prefrontal circuit dysfunction by

- antidepressant-induced spine formation. *Science*, 2019, 364, pii: eaat8078. doi: 10.1126/science.aat8078. [PubMed: 30975859]
28. Cameron LP; Olson DE Dark Classics in Chemical Neuroscience: *N,N*-Dimethyltryptamine (DMT). *ACS Chem. Neurosci*, 2018, 9, 2344–2357. [PubMed: 30036036]
 29. Warnault V; Darceq E; Levine A; Barak S; Ron D Chromatin remodeling--a novel strategy to control excessive alcohol drinking. *Transl. Psychiatry*, 2013, 3, e231. doi: 10.1038/tp.2013.4. [PubMed: 23423140]
 30. Glick S; Kuehne M; Raucci J; Wilson T; Larson D; Keller R; Carlson J Effects of Iboga Alkaloids on Morphine and Cocaine Self-Administration in Rats: Relationship to Tremorigenic Effects and to Effects on Dopamine Release in Nucleus Accumbens and Striatum. *Brain Res*, 1994, 657, 14–22. [PubMed: 7820611]
 31. Giannotti G; Barry SM; Siemsen BM; Peters J; McGinty JF Divergent Prelimbic Cortical Pathways Interact with BDNF to Regulate Cocaine-seeking. *J. Neurosci*, 2018, 38, 8956–8966. [PubMed: 30185459]
 32. Glick SD; Kuehne ME; Maisonneuve IM; Bandarage UK; Molinari HH 18-Methoxycoronaridine, a Non-Toxic Iboga Alkaloid Congener: Effects on Morphine and Cocaine Self-Administration and on Mesolimbic Dopamine Release in Rats. *Brain Res*, 1996, 719, 29–35. [PubMed: 8782860]
 33. Carnicella S; He DY; Yowell QV; Glick SD; Ron D Noribogaine, but not 18-MC, exhibits similar actions as ibogaine on GDNF expression and ethanol self-administration. *Addict. Biol*, 2010, 15, 424–433. [PubMed: 21040239]
 34. Bandarage UK; Kuehne ME; Glick SD Total Syntheses of Racemic Albifloranine and Its Anti-Addictive Congeners, Including 18-Methoxycoronaridine. *Tetrahedron*, 1999, 55, 9405–9424.
 35. Langheinrich U1; Vacun G; Wagner T Zebrafish embryos express an orthologue of HERG and are sensitive toward a range of QT-prolonging drugs inducing severe arrhythmia. *Toxicol. Appl. Pharmacol*, 2003, 193, 370–382. [PubMed: 14678746]
 36. Sampurna BP; Audira G; Juniardi S; Lai Y-H; Hsiao C-D A Simple ImageJ-Based Method to Measure Cardiac Rhythm in Zebrafish Embryos. *Inventions*, 2018, 3, 21 10.3390/inventions3020021
 37. Westerfield M (2007) *THE ZEBRAFISH BOOK*, 5th Edition; A guide for the laboratory use of zebrafish (*Danio rerio*), Eugene, University of Oregon Press).
 38. Ahrens MB; Orger MB; Robson DN; Li JM; Keller PJ Whole-brain functional imaging at cellular resolution using light-sheet microscopy. *Nat. Methods*, 2013, 10, 413–420. [PubMed: 23524393]
 39. Kroeze WK; Sassano MF; Huang XP; Lansu K; McCorvy JD; Giguère PM; Sciaky N; Roth BL PRESTO-Tango as an open-source resource for interrogation of the druggable human GPCRome. *Nat. Struct. Mol. Biol*, 2015, 22, 362–369. [PubMed: 25895059]
 40. Barupal DK; Zhang Y; Shen T; Fan S; Roberts BS; Fitzgerald P; Wancewicz B; Valdiviez L; Wohlgemuth G; Byram G; Choy YY; Haffner B; Showalter MR; Vaniya A; Bloszies CS; Folz JS; Kind T; Flenniken AM; McKerlie C; Nutter LMJ; Lloyd KC; Fiehn O A Comprehensive Plasma Metabolomics Dataset for a Cohort of Mouse Knockouts within the International Mouse Phenotyping Consortium. *Metabolites*, 2019, 9 pii: E101. doi: 10.3390/metabo9050101. [PubMed: 31121816]
 41. Feng G; Mellor RH; Bernstein M; Keller-Peck C; Nguyen QT; Wallace M; Nerbonne JM; Lichtman JW; Sanes JR Imaging neuronal subsets in transgenic mice expressing multiple spectral variants of GFP. *Neuron*, 2000, 28, 41–51. [PubMed: 11086982]
 42. Xu T; Yu X; Perlik AJ; Tobin WF; Zweig JA; Tennant K; Jones T; Zuo Y Rapid formation and selective stabilization of synapses for enduring motor memories. *Nature*, 2009, 462, 915–919. [PubMed: 19946267]
 43. Chen CC; Lu J; Yang R; Ding JB; Zuo Y Selective activation of parvalbumin interneurons prevents stress-induced synapse loss and perceptual defects. *Mol. Psychiatry*, 2018, 23, 1614–1625. [PubMed: 28761082]
 44. Vazquez M; Frazier JH; Reichel CM; Peters J Acute ovarian hormone treatment in freely cycling female rats regulates distinct aspects of heroin seeking. *Learn. Mem*, 2019, 27, 6–11. [PubMed: 31843977]

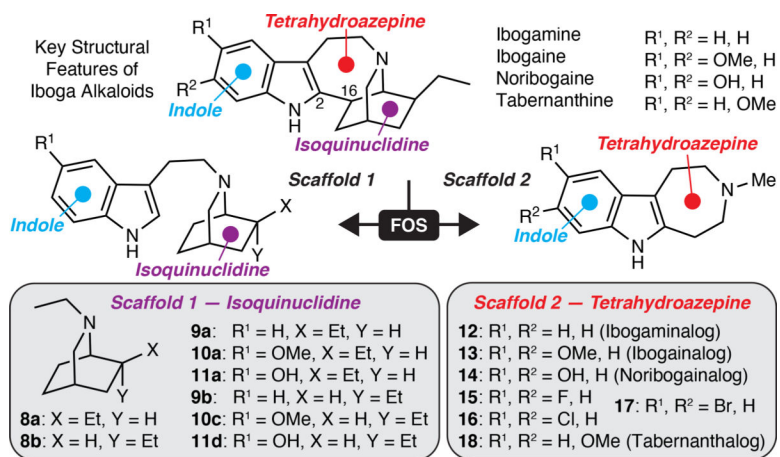


Figure 1. Function-oriented synthesis of ibogalogs.

(a) Key structural features of ibogaine, related alkaloids, and ibogalogs.

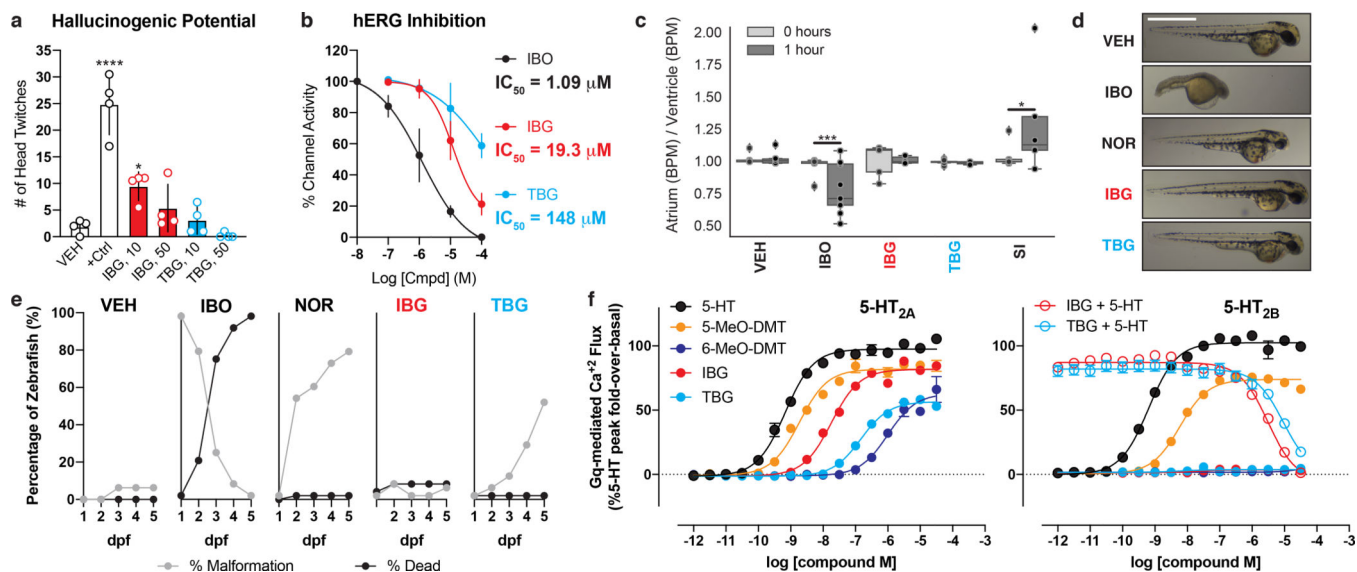


Figure 2. TBG is a safer analog of iboga alkaloids.

(a) Mouse HTR assays demonstrate that TBG is not hallucinogenic. The doses (mg/kg) of IBG and TBG are indicated. +Ctrl = 5-MeO-DMT (10 mg/kg). (b) Inhibition of hERG channels expressed in HEK293 cells. Error bars represent SD. (c) Unlike ibogaine, IBG and TBG do not increase the risk for arrhythmias in larval zebrafish. Sertindole (SI) was used as a positive control. (d) Representative images of zebrafish treated with compounds (100 μ M) for 2 dpf. Scale bar = 1 mm. (e) Compound-induced malformation and death over time ($n = 48$ zebrafish for all treatment groups). (f) Activities at 5-HT_{2A} and 5-HT_{2B} receptors as measured by Gq-mediated calcium flux. Data represent percent 5-HT fold-over-basal response. Exact N numbers for each experimental condition are reported in the Source Data and Supplementary Table 1. Specific statistical tests, information on reproducibility, and exact p values are reported in the Methods and Supplementary Table 1.

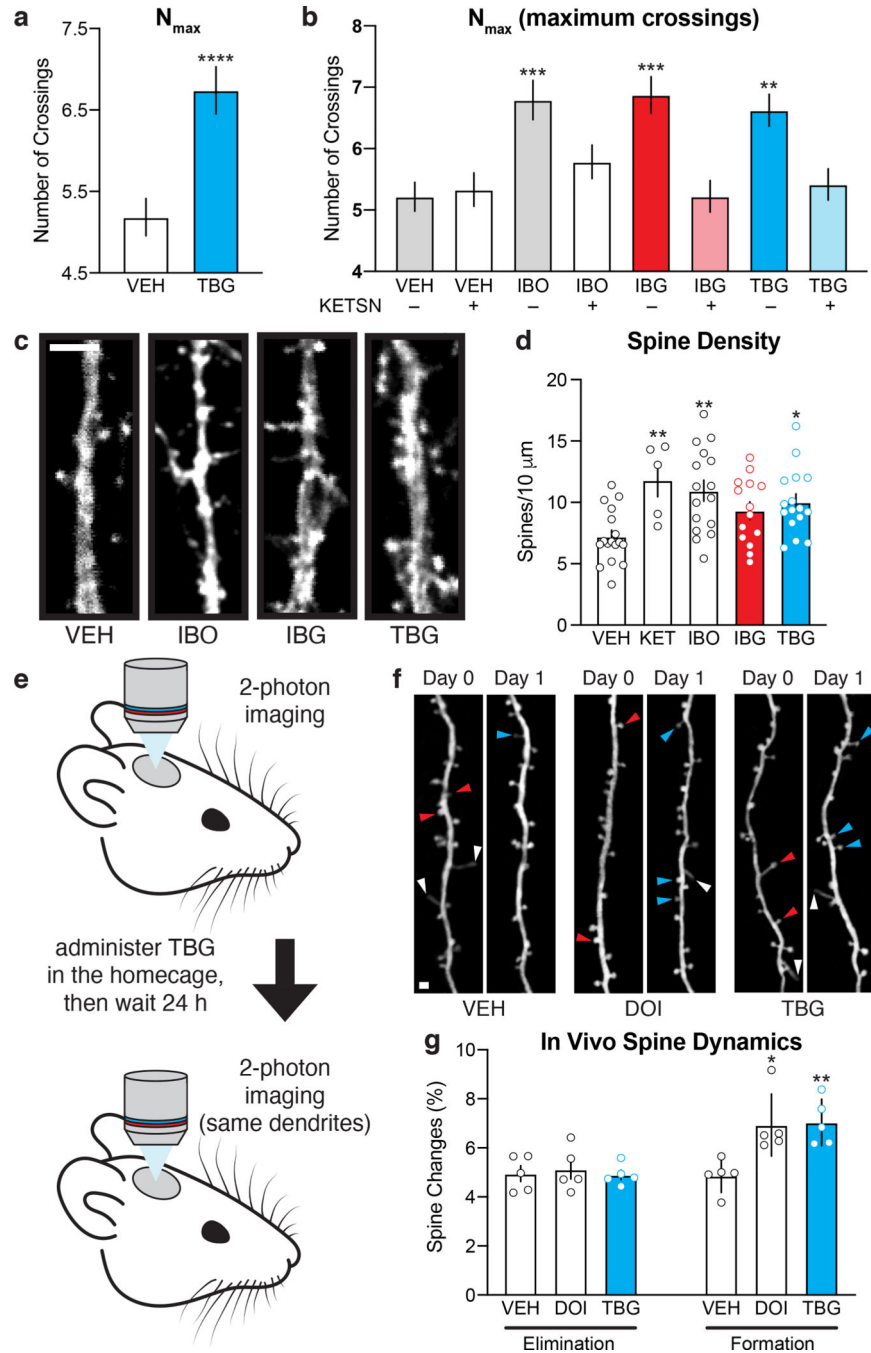


Figure 3. TBG promotes neural plasticity.

(a) Maximum numbers of crossings (N_{max}) of Sholl plots obtained from rat embryonic cortical neurons (DIV6). (b) The effects of TBG on dendritic growth are blocked by the 5-HT_{2A} antagonist ketanserin. (c) Representative images of secondary branches of rat embryonic cortical neurons (DIV20) after treatment with ibogalogs for 24 h. Scale bar = 2 μ m. (d) TBG increases dendritic spine density on rat embryonic cortical neurons (DIV20) after treatment for 24 h. (e) Schematic illustrating the design of transcranial 2-photon imaging experiments. (f) Representative images of the same dendritic segments from mouse

primary sensory cortex before (Day 0) and after (Day 1) treatment. Blue, red, and white arrowheads represent newly formed spines, eliminated spines, and filopodia, respectively. Scale bar = 2 μm . (g) DOI and TBG increase spine formation but have no effect on spine elimination. Exact N numbers for each experimental condition are reported in the Source Data and Supplementary Table 1. Specific statistical tests, information on reproducibility, and exact p values are reported in the Methods and Supplementary Table 1.

Author Manuscript

Author Manuscript

Author Manuscript

Author Manuscript

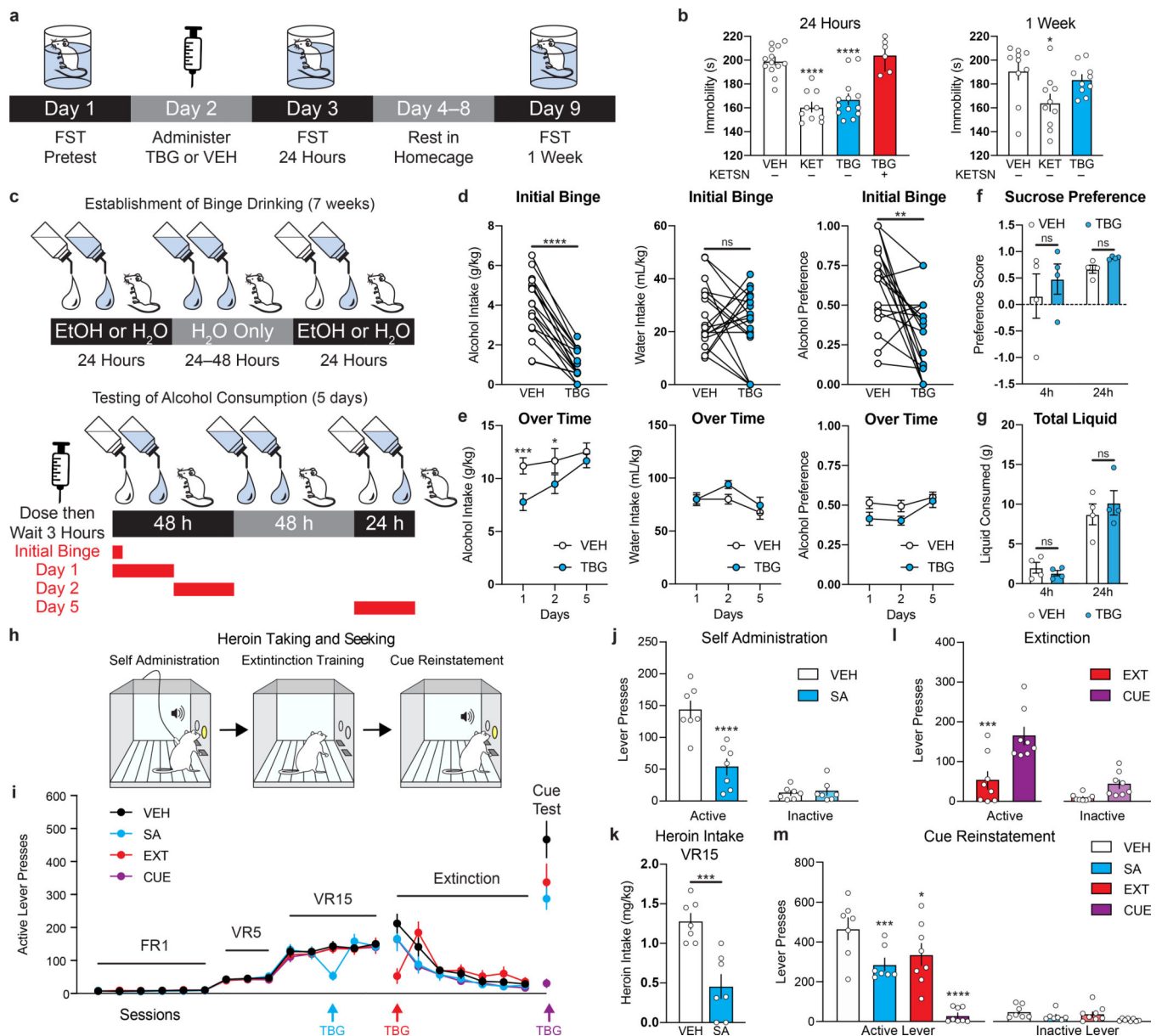


Figure 4. Effects of TBG on animal behaviors relevant to depression, AUD, and SUD.

(a) Schematic illustrating the design of FST experiments conducted without UMS. (b) The antidepressant-like effects of TBG are blocked by ketanserin. (c) Timeline of alcohol binge-drinking experiment. White and blue droplets represent 20% EtOH and H₂O, respectively. (d) TBG acutely reduced EtOH consumption and preference during a binge drinking session without impacting H₂O intake. (e) Acute TBG administration decreased EtOH consumption for at least 48 h. (f–g) TBG did not decrease sucrose preference (f) or reduce total liquid consumption (g) in a two-bottle choice experiment. (h) Schematic illustrating the design of the heroin self-administration experiments. (i) Heroin seeking over time is shown. Colored arrows indicate when each group received TBG. VEH was administered at all other time points to each group. (j–k) TBG acutely reduced heroin self-administration—both lever pressing (j) and heroin intake (k). (l) TBG acutely reduced heroin-seeking when

administered immediately before the first extinction session. The CUE (injection 1 = VEH, injection 2 = VEH) and EXT (injection 1 = VEH, injection 2 = TBG) groups were compared, as they were matched for the number of withdrawal days between the last self-administration and first extinction session. (m) Acute TBG completely blocked cued reinstatement (purple bar, CUE). A single prior (12–14 d) administration of TBG during heroin self-administration or the first day of extinction (blue and red bars, respectively) inhibited cued reinstatement. Exact N numbers for each experimental condition are reported in the Source Data and Supplementary Table 1. Specific statistical tests, information on reproducibility, and exact p values are reported in the Methods and Supplementary Table 1.

Author Manuscript

Author Manuscript

Author Manuscript

Author Manuscript